USGS-OFR-92-201

U.S. DEPARTMENT OF THE INTERIOR

U.S. GEOLOGICAL SURVEY

Water permeability and related rock properties measured on core samples from the Yucca Mountain USW GU-3/G-3 and USW G-4 boreholes, Nevada Test Site, Nevada

By

Lennart A. Anderson[1]

Open-File Report 92-201

[1]U.S.Geological Survey, Box 25046 Federal Center, MS 964, Denver, CO 80225-0046

Contents

Water permeability and related rock properties measured on core samples from the Yucca Mountain USW GU-3/G-3 and USW G-4 boreholes, Nevada Test Site, Nevada

by

Lennart A. Anderson
U.S. Geological Survey
Denver, Colorado 80225

ABSTRACT

Core samples from the Yucca Mountain USW GU-3/G-3 and USW G-4 boreholes were measured for bulk density, grain density, porosity, resistivity, and water permeability as part of a comprehensive geologic investigation designed to determine the suitability of Yucca Mountain as a site for the containment of high-level radioactive waste products. The cores were selected at the drill sites so as to be representative of the major lithologic variations observed within stratigraphic units of the Paintbrush Tuff, Calico Hills Tuff, Crater Flat Tuff, Lithic Ridge Tuff, and Older Tuffs. USW GU-3/G-3 was drilled to a depth of 1533.8 meters and the USW G-4 borehole penetrated to the 914.7 meter level. Two hundred and twenty six samples were used in the laboratory study of which two hundred were sample pairs drilled from a common core. The paired samples were oriented axially and perpendicular to the alignment of the borehole.

Dry and saturated bulk density, grain density, and porosity measurements were made on the core samples principally to establish that a reasonable uniformity exists in the textural and mineral character of the sample pairs. Where bulk densities are different, grain density data show that the disparities can usually be attributed to porosity variations rather than to inequalities in mineral content. Electrical resistivity measured on sample pairs tended to be lower along the plane transverse to the vertical axis of the drill core herein referred to as the horizontal plane. Permeability values, ranging from virtually 0 (<.02 microdarcies) to over 200 millidarcies, also indicate a preferential flow direction along the horizontal plane of the individual tuff units. Of the 67 sample pairs from the USW GU-3/G-3 borehole, 58 percent of the horizontally oriented core had a higher permeability and lower resistivity than their vertically oriented counterparts. Only in 10 percent of the 67 sample pairs did the vertical core demonstrate a similar permeability/resistivity relationship. In those sample pairs from the USW G-4 borehole, 65 percent of the horizontal plugs and 24 percent of the vertical plugs exhibited this same permeability/resistivity correspondence. Despite the non-bedded character of the ash-flow tuffs, the welding process possibly produced an interconnecting pore structure along the implied bedding plane so as to provide a continuous and less tortuous path for both current and water flow. Permeability decreases with flow duration in all but the non-welded tuffs as unconsolidated particles within the pore network are repositioned so as to impede the continued flow of water through the rock. Reversing flow direction initially restores the permeability of the rock to its original or maximum value.

INTRODUCTION

Permeability measurements have been made on core samples from the Yucca Mountain USW GU-3/G-3 and USW G-4 boreholes to determine relative levels of fluid conductivity attributable to the matrix of the tuffs encountered within

the respective boreholes. The samples were in the form of cylinders, 2.54 cm in length and diameter, removed from larger volume core originally used in a rock property study by Anderson, 1984. Wherever possible, samples were collected in pairs in order to simulate vertical and horizontal flow conditions. The distance between the volumetric centers of the sample pairs was about 3.0 cm. Because of the orientation of open fractures or structural incompetence, not all samples were suitable for the measurement.

Dry and saturated bulk density, grain density, and porosity were also made on the sample pairs to determine the variability in the homogeneity of the core in terms of texture and mineral content as a possible guide to the understanding of permeability differences found amongst sample pairs. Electrical resistivity was measured on the paired core samples specifically to determine the orientation of the preferential current flow path through the rock and its correspondence to the direction of maximum water flow. Resistivity in itself can sometimes be used as an estimator of the permeability of a rock (Brace, 1977).

Yucca Mountain, composed of a series of northerly aligned structural blocks (Carr and others, 1986), is located adjacent to the southwest border of the Nevada Test Site (NTS) in the Topopah Spring SW Quadrangle, Nevada (figure 1). The blocks consist of nonwelded to densely welded ash-flow and ash-fall bedded tuffs. Also shown are the locations of the USW GU-3/G-3 and USW G-4 boreholes within the Yucca Mountain complex. The geologic character of Yucca Mountain is currently under study as part of the Nevada Nuclear Waste Storage Investigations (NNWSI) project designed to identify suitable underground repositories for radioactive waste products.

As the letter designation implies, USW GU-3/G-3 refers to two boreholes with G-3 being displaced approximately 30 meters north-northwest of the GU-3 location. GU-3 was drilled to 806.1 meters and G-3 continued to a depth of 1533.8 meters. Because of their close proximity, the rock property data obtained on the borehole core have been treated as having originated from a single continuous drillhole.

The stratigraphic sequence, lithology, and other descriptions pertaining to the USW GU-3/G-3 borehole, hereafter referred to as G-3, are taken from the work of Scott and Castellanos (1984). In descending order, the borehole penetrated the Tiva Canyon and Topopah Spring Members of the Paintbrush Tuff; the Calico Hills Tuff; the Crater Flat Tuff, composed of the Prow Pass Member, the Bullfrog Member, and the Tram Member; Lithic Ridge Tuff; and Older Tuffs. The rocks are Miocene in age (Carr and others, 1984).

The stratigraphy, lithology, and miscellaneous details pertaining to borehole USW G-4 (G-4) have been described by Spengler and Chornack, 1984. G-4 was cored to a depth of 914.7 meters penetrating the same section described for G-3 but terminating in the Tram Member of the Crater Flat Tuff. A relatively thin section of the Pah Canyon Member of the Paintbrush Tuff was also identified. Several bedded tuff intervals were penetrated in both boreholes.

The principal purpose of the investigation was to determine the matrix permeability of the tuff samples. A secondary objective was to test for a preferential flow path for water migration through the pore spaces of the rock through the use of vertically and horizontally oriented sample pairs. A third goal was to evaluate the permeability variations against differences in mineral content and texture within the paired samples, as deduced from grain

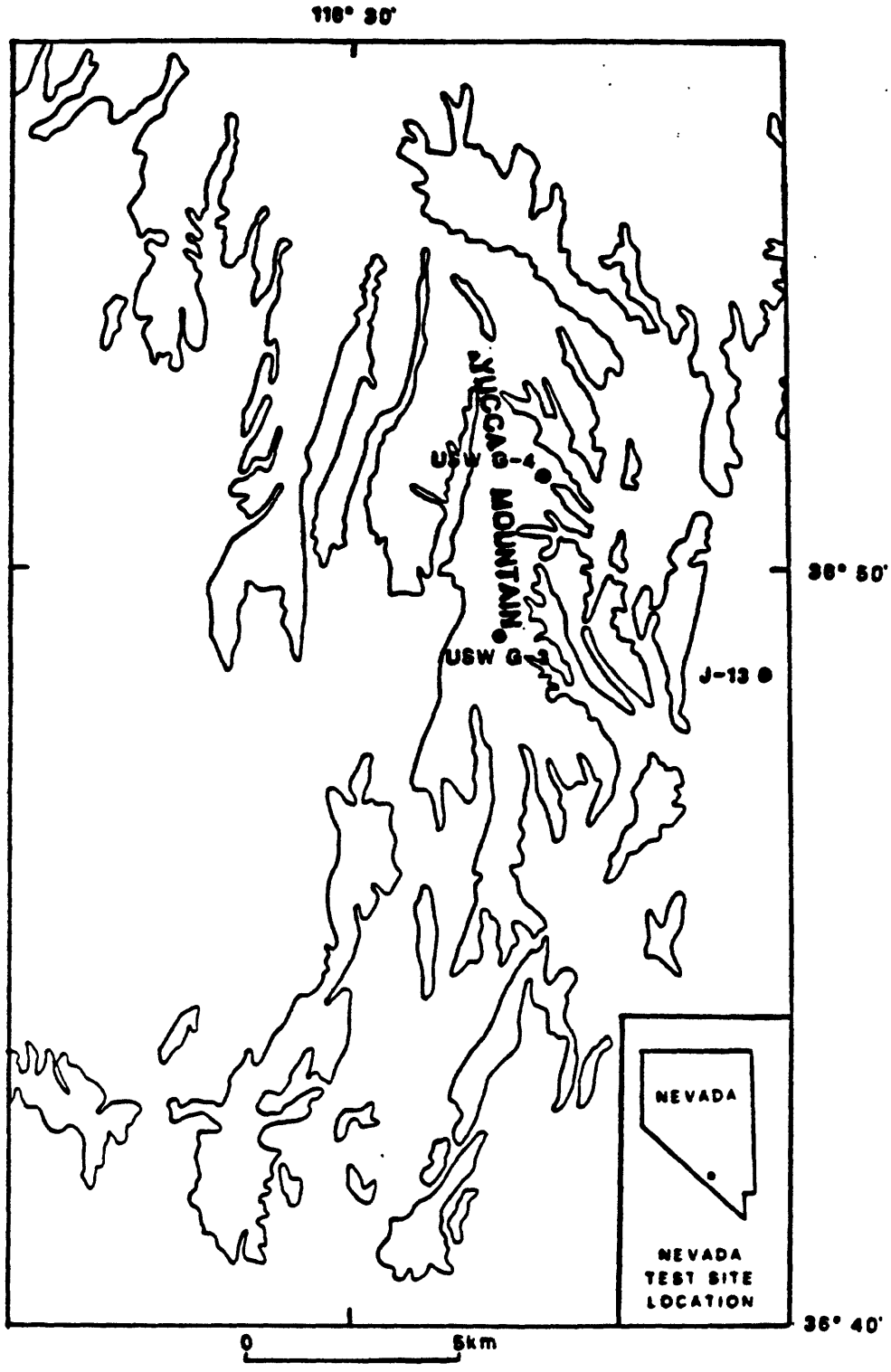

Figure 1. Map of the Yucca Mountain study area showing the locations of the USW GU-3/G-3 and USW G-4 boreholes and the J-13 water drillhole.

density and porosity measurements. A fourth goal was to measure the resistivity of the samples in order to determine if the preferential current flow path follows that of water flow.

According to Winograd and Thordarson, 1975, water movement through the densely welded Tiva Canyon and Topopah Spring Members of the Paintbrush Tuff is by means of primary (cooling) and secondary fractures. Interstitial permeability is considered to be negligible in these tuffs. Within the Calico Hills Tuff and the three Members of the Crater Flat Tuff fractures are believed to be poorly connected, therefore, ground water movement is primarily through the pore connections of the rock. With the knowledge that, in the latter group, matrix permeability is a factor in both ground water migration and meteoric water infiltration in the Yucca Mountain environment, the potential for radioactive waste transport by means of matrix permeability necessitated the determination of the permeabilities of the available samples.

Density, porosity, and resistivity measurements

The manner in which density, porosity, and resistivity measurements were made is described in Anderson, 1981. Values of saturated bulk density (SBD); dry bulk density (DBD); grain density (GD); and water-accessible porosity, (ϕ), were calculated as follows:

SBD = Ws/Vb, where Ws is the weight of the saturated sample and Vb is the bulk volume of the sample as determined by the difference between Ws and Wsp, the weight of the sample suspended in distilled water. The difference is divided by the density of the water at ambient temperature.

DBD = Wd/Vb, where Wd is the dry weight of the sample.

GD = $Wd*\sigma/(Wd - Wsp)$, where σ is the density of distilled water at ambient temperature.

$\phi = (Ws - Wd)/Vb$.

Density units are presented in megagrams per cubic meter (Mg/m^3) which is numerically equivalent to grams per cubic centimeter (g/cc).

The electrical resistance of the samples, saturated with 14.5 ohm-m tap water, was measured at a frequency of 100 hertz using a Hewlett-Packard digital LCR meter and a four-electrode sample holder. Resistance was converted to resistivity using sample length and diameter caliper measurements by the equation

$$\rho = RA/l$$

where ρ is the sample resistivity in ohm-meters, R is the electrical resistance in ohms, and A and l are the cross-sectional area and length of the sample, respectively.

Density, porosity, and resistivity values of the USW GU-3/G-3 borehole samples

Horizontal and vertical permeability measurements were not made on the same sample but rather on sample pairs drilled from the single specimens of drill core used in the rock property study reported by Anderson, 1984. Therefore, it was considered important to test for variations in the texture and mineral content of the groundmass as a factor in controlling fluid flow through the samples. Grain density and porosity data are best suited to that

purpose. In the process of obtaining grain density and porosity data, however, dry and saturated bulk density values for the core samples were also acquired (figures 2 and 3, respectively). The sample density values are listed in Table 1 in the Appendix. Dry bulk density and saturated bulk density plots demonstrate the range of density values to be expected within the borehole depending on the degree of water saturation within the rock. Density variations within and between stratigraphic units are the result of differences in welding, mineral content, and textural changes. Examination of the paired data points in each illustration indicate that most bulk density values are in close agreement (within 0.02 Mg/m^3), but locally, disparities as high as 0.22 Mg/m^3 can be found in the dry bulk density data caused primarily by porosity differences.

The grain density values plotted in figure 4 indicate very little difference in the mineral content of the sample pairs. Where small differences are evident, the cause may be attributed to clay/zeolite alteration commonly associated with the higher porosity non-welded tuff. An example of a relatively large sample pair mineral dissimilarity occurs within the sample from the 201.3 m depth. The vertically oriented sample has a substantially higher grain density than the horizontal sample. The larger volume measurement reported in Anderson, 1984, was 2.58 Mg/m^3, a value approximately midway between the 2.709 and 2.493 Mg/m^3 values obtained on the smaller samples. It is likely that thinly layered, relatively dense phenocrysts, possibly pyroxene (3.2-3.6 Mg/m^3) and biotite (2.9 Mg/m^3) as described in Scott and Castellanos, 1984, have been incorporated into the vertical sample so as to produce its unusually high grain density.

The paired sample porosity values listed in Table 2 in the Appendix and shown in figure 5 vary as a function of the degree to which the tuffs have been welded. Low porosities are associated with densely-welded tuffs and, conversely, the higher porosities relate to non-welded and ash-fall bedded tuffs. In that the grain density data indicate a rather uniform mineral content between virtually all the individual sets of paired samples, it seems evident that porosity variations between these same sample sets are the cause of the disparities recorded in the bulk density plots. There is no discernable pattern in the porosity differences between paired samples in that no one sample orientation demonstrates a consistently higher porosity than the other.

Resistivity values determined for all available samples are listed in Table 2 in the Appendix and plotted in figure 6. The higher resistivities are associated with densely welded tuffs whereas the lower resistivities correlate with ash-fall and non-welded tuffs.

Seventy sample pairs were included in the resistivity study. Of these, 44 horizontally oriented samples had resistivities lower (by more than ten percent) than the resistivity of their vertical counterparts. In contrast, only 6 vertically oriented samples had resistivities less than their horizontal counterparts. The remaining 20 sample pairs were essentially equal in resistivity. The coefficient of resistivity anisotropy varies from 1 to slightly less than 3 for the entire sample set.

Keller and Frischknecht, 1966, state that the longitudinal (horizontal) resistivity is always less than the transverse (vertical) resistivity for layered or bedded rock. According to Winograd and Thordarson, 1975, the ash-flow tuffs at the Nevada Test Site are characteristically non-sorted and exhibit no bedding. Nevertheless, the data imply that some level of

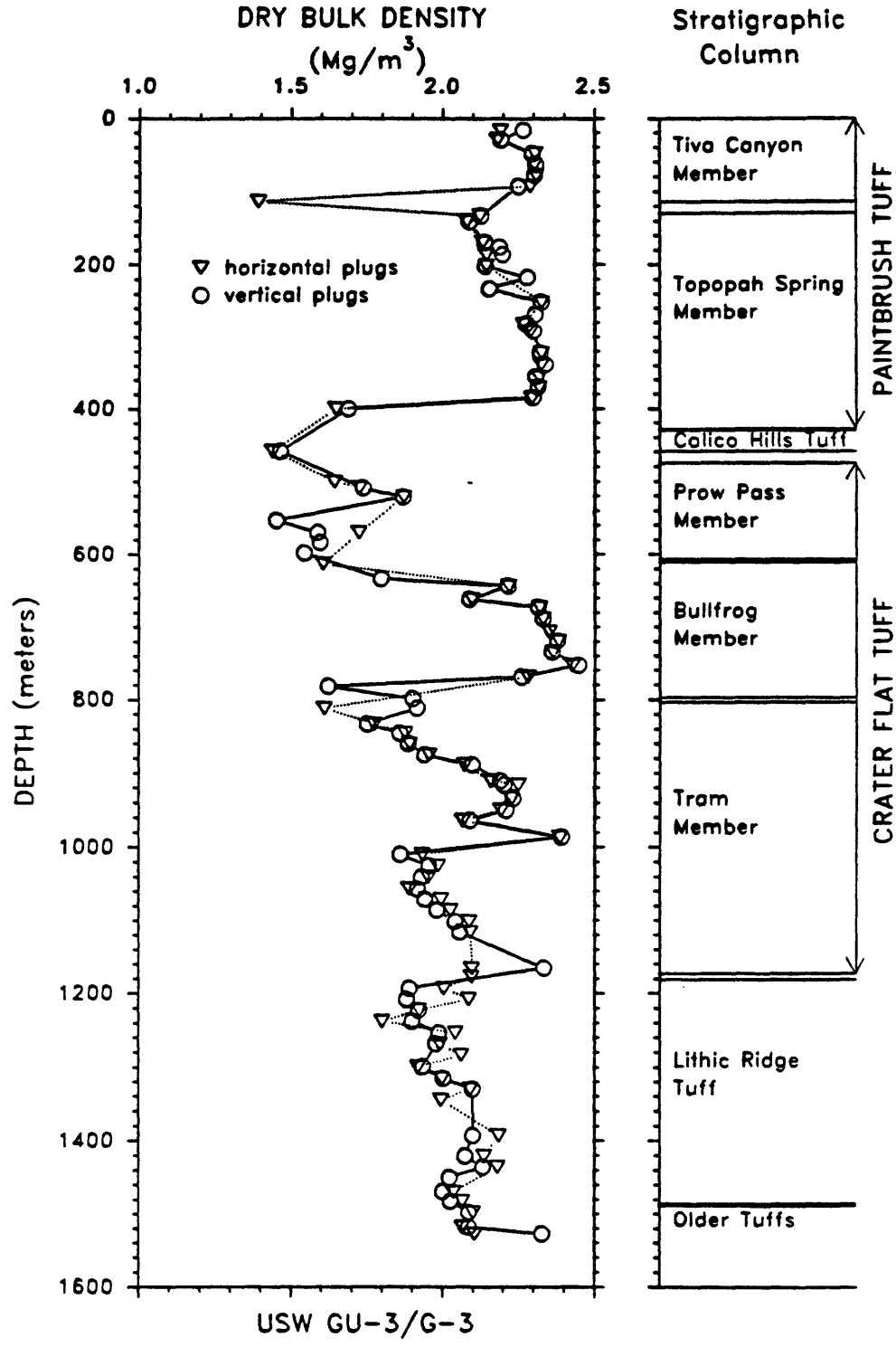

Figure 2. Dry bulk density values for USW GU-3/G-3 horizontally and vertically oriented samples plotted as a function of sampling depth. The unlabeled intervals in the stratigraphic column are bedded ash-fall tuffs (Scott and Castellanos, 1984).

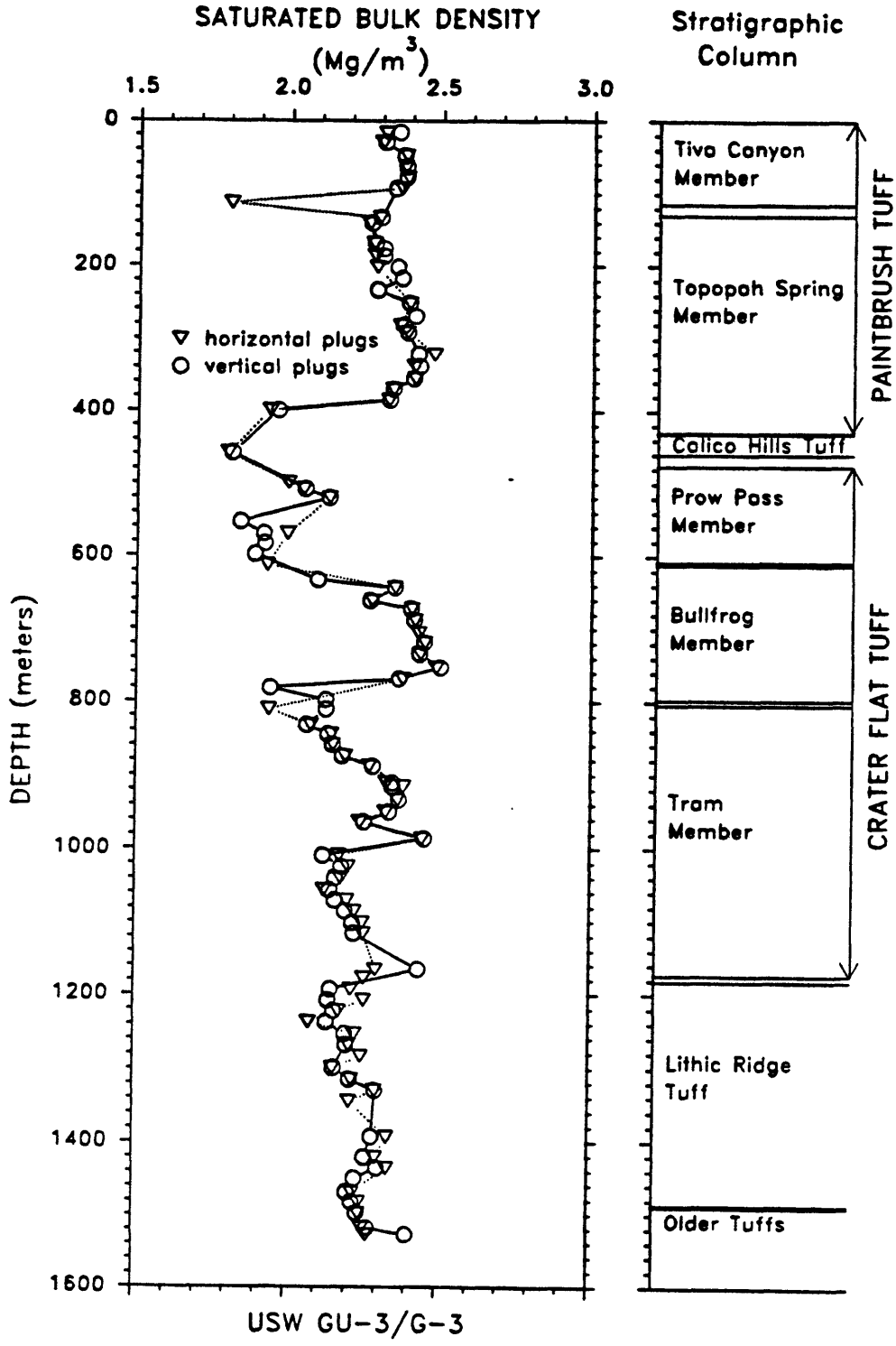

Figure 3. Saturated bulk density values for USW GU-3/G-3 horizontally and vertically oriented samples plotted as a function of sampling depth. The unlabeled intervals in the stratigraphic column are bedded ash-fall tuffs (Scott and Castellanos, 1984).

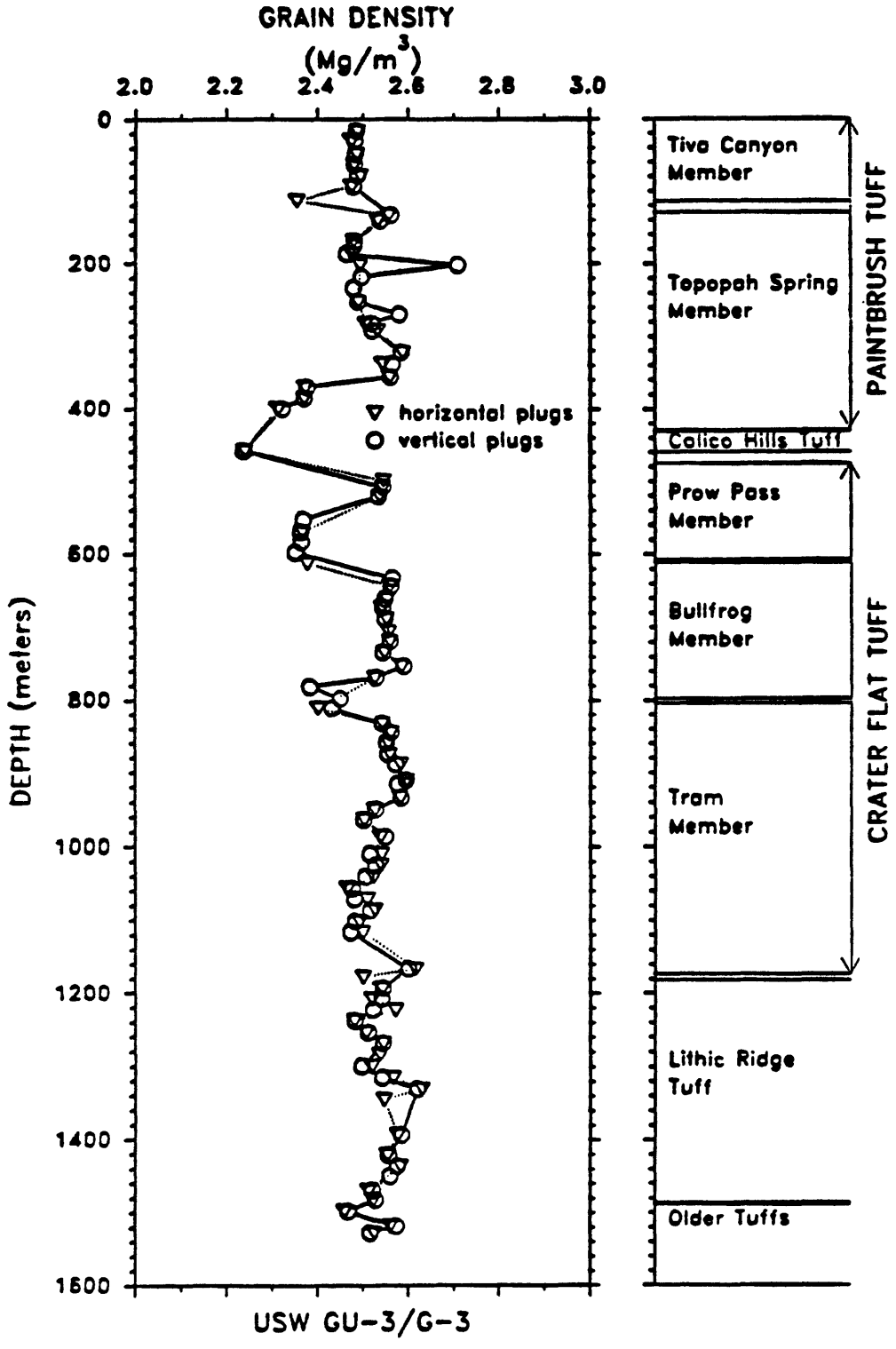

Figure 4. Grain density values for USW GU-3/G-3 horizontally and vertically oriented samples plotted as a function of sampling depth. The unlabeled intervals in the stratigraphic column are bedded ash-fall tuffs (Scott and Castellanos, 1984).

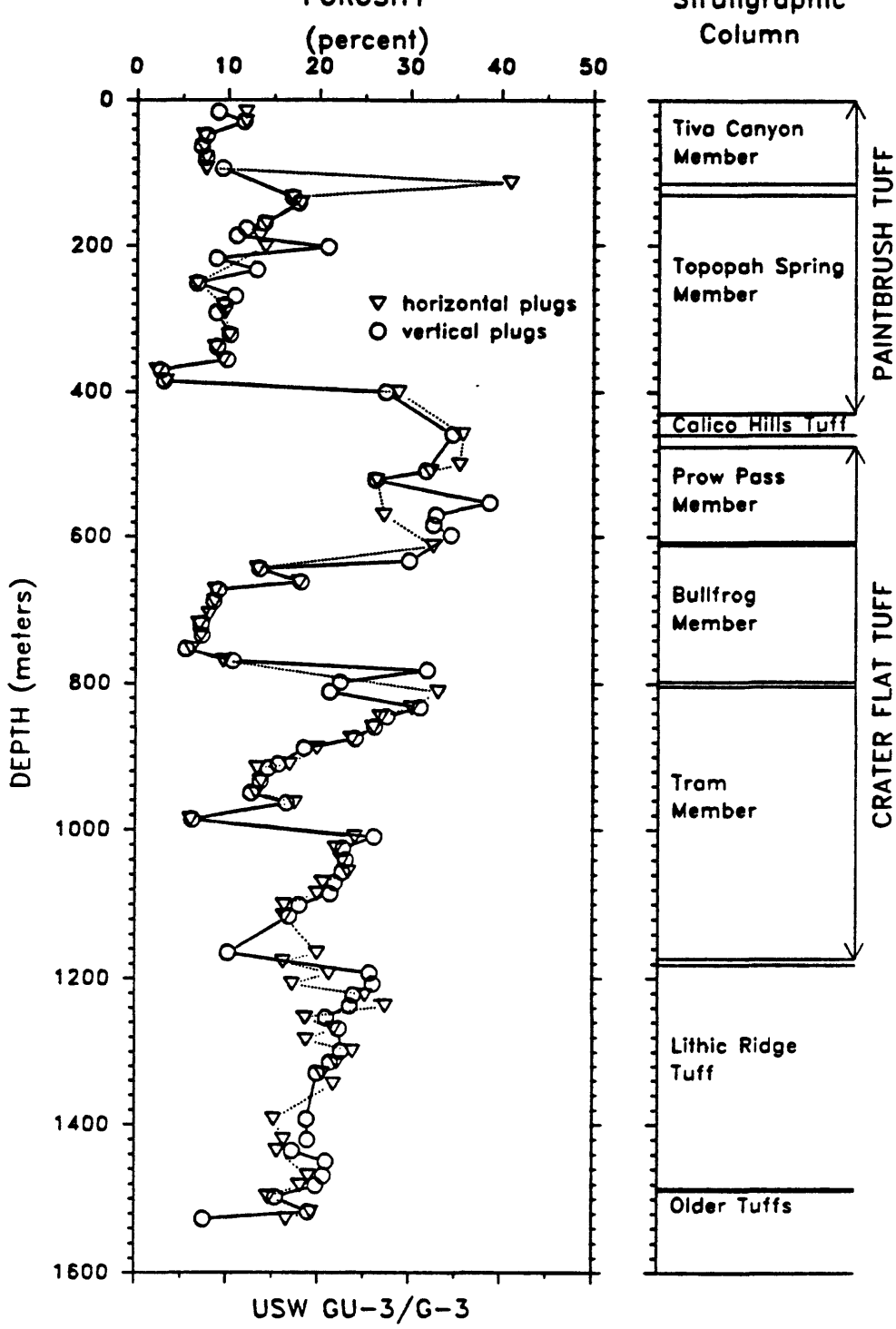

Figure 5. Porosity values for USW GU-3/G-3 horizontally and vertically oriented samples plotted as a function of sampling depth. The unlabeled intervals in the stratigraphic column are bedded ash-fall tuffs (Scott and Castellanos, 1984).

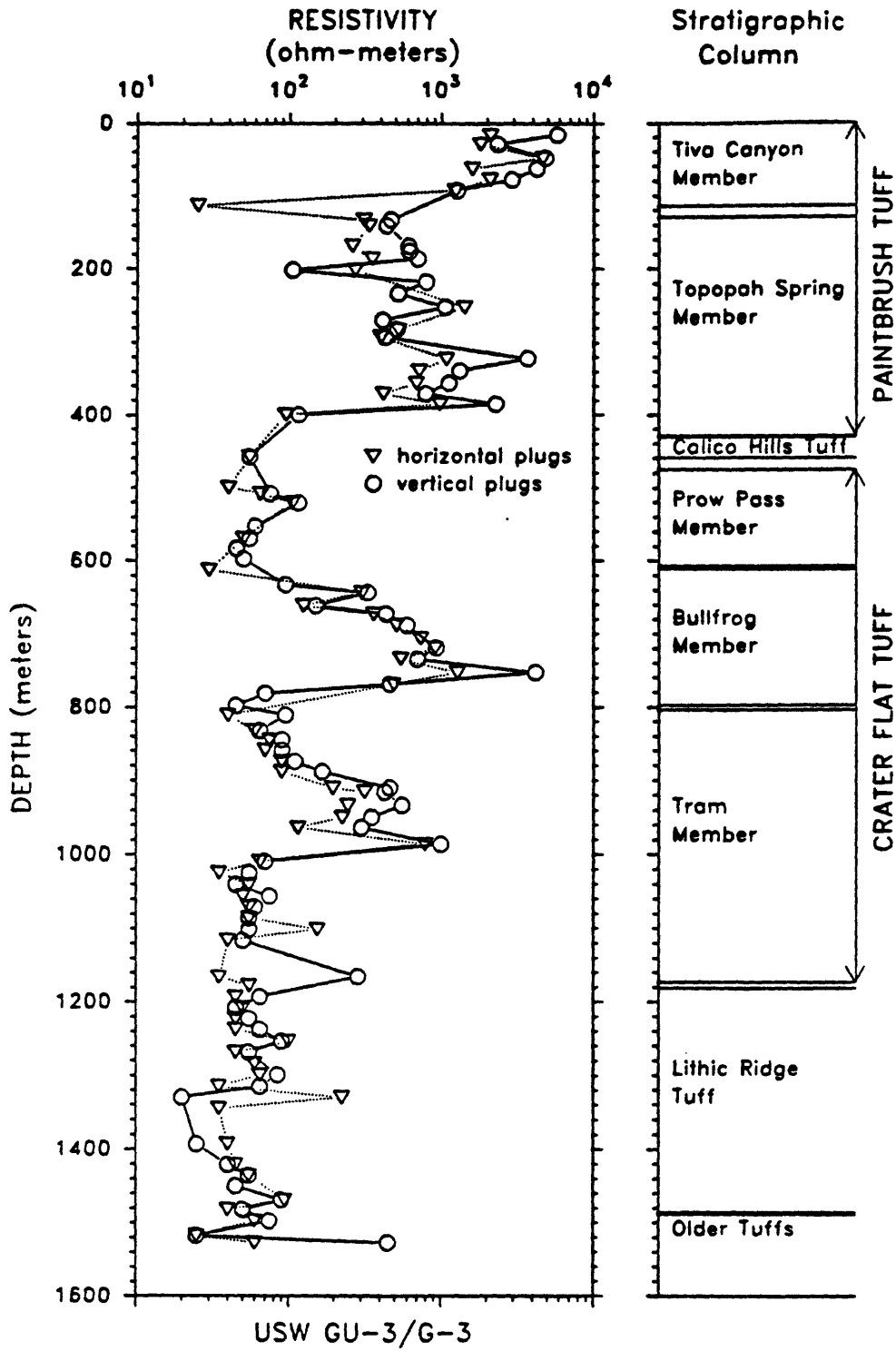

Figure 6. Resistivity values for USW GU-3/G-3 horizontally and vertically oriented samples plotted as a function of sampling depth. The unlabeled intervals in the stratigraphic column are bedded ash-fall tuffs (Scott and Castellanos, 1984).

preferential pore alignment has developed following deposition of the tuffs, principally in the horizontal plane. Evidence of an enhanced electrical current flow through the rock along a discreet path may also be an indicator of the direction water might be expected to flow through the rock matrix.

Several investigators have utilized resistivity data to estimate the permeability of a specific rock with good results (e.g., Brace and others, 1968). The calculation is based on a knowledge of the conductivity of the introduced, highly saline, pore water which is sufficient to suppress the contribution high ion exchange minerals may add to the resistivity of the rock. There is a sufficient amount of clays and zeolites in the Yucca Mountain tuffs, particularly in the less welded sections, to consider that these minerals are a contributing factor in controlling the resistivity of the rock. Without knowledge of the mineral content of the rock, particularly with regard to alteration products, any attempt at correlating resistivity with permeability would therefore be judged unreliable for this set of tuff samples.

Density, porosity, and resistivity values for USW G-4 borehole samples

Bulk and grain density values for the G-4 borehole samples are listed in Table 3, and porosity and resistivity values are listed in Table 4. The tables are included in the Appendix.

Dry and saturated bulk density data plots are shown in figures 7 and 8, respectively. Density values for the paired samples from the Calico Hills Tuff and the Crater Flat Tuff are virtually the same, but within the Paintbrush Tuff, deviations in density values between the sample pairs are more evident. Grain density values for the individual sample pairs are comparable indicating that within each sample set the mineral content is essentially the same (figure 9). The porosity plot (figure 10) shows paired sample values varying in the same manner as the bulk densities.

The porosity data indicates the greatest differences in paired sample values occur within the interval defined by the Topopah Spring Member. Elsewhere, with some exceptions, the porosity correspondence between paired sample values is within a few percent. As with the G-3 samples there is no pattern established by sample orientation in the porosities determined for the Topopah Spring core. Possibly, a random distribution of lithophysal cavities within the Topopah Spring Tuff is responsible for the differences observed in sample pair porosities. Lithophysal cavities are common within the Topopah Spring Member (Spengler and Chornack, 1984), however, the samples were taken so as to deliberately minimize the presence of such cavities within the measured core.

Resistivity values determined for the G-4 sample pairs are plotted in figure 11. Of the 30 sample paris measured, 19 vertically oriented cores had resistivities more than 10 percent higher than their horizontal counterparts. In only 3 other sample pairs did the opposite result occur. Eight sample pairs produced essentially the same resistivities. Sample pair resistivities are more likely to be the same when less than 100 ohm-m. As resistivity increases with increased welding, the lower porosity and smaller pore size adds to the tortuosity of the current flow path nonuniformly so as to produce a divergence in paired sample resistivities. The horizontal alignment of the pore structure developed during the welding process is believed to be the

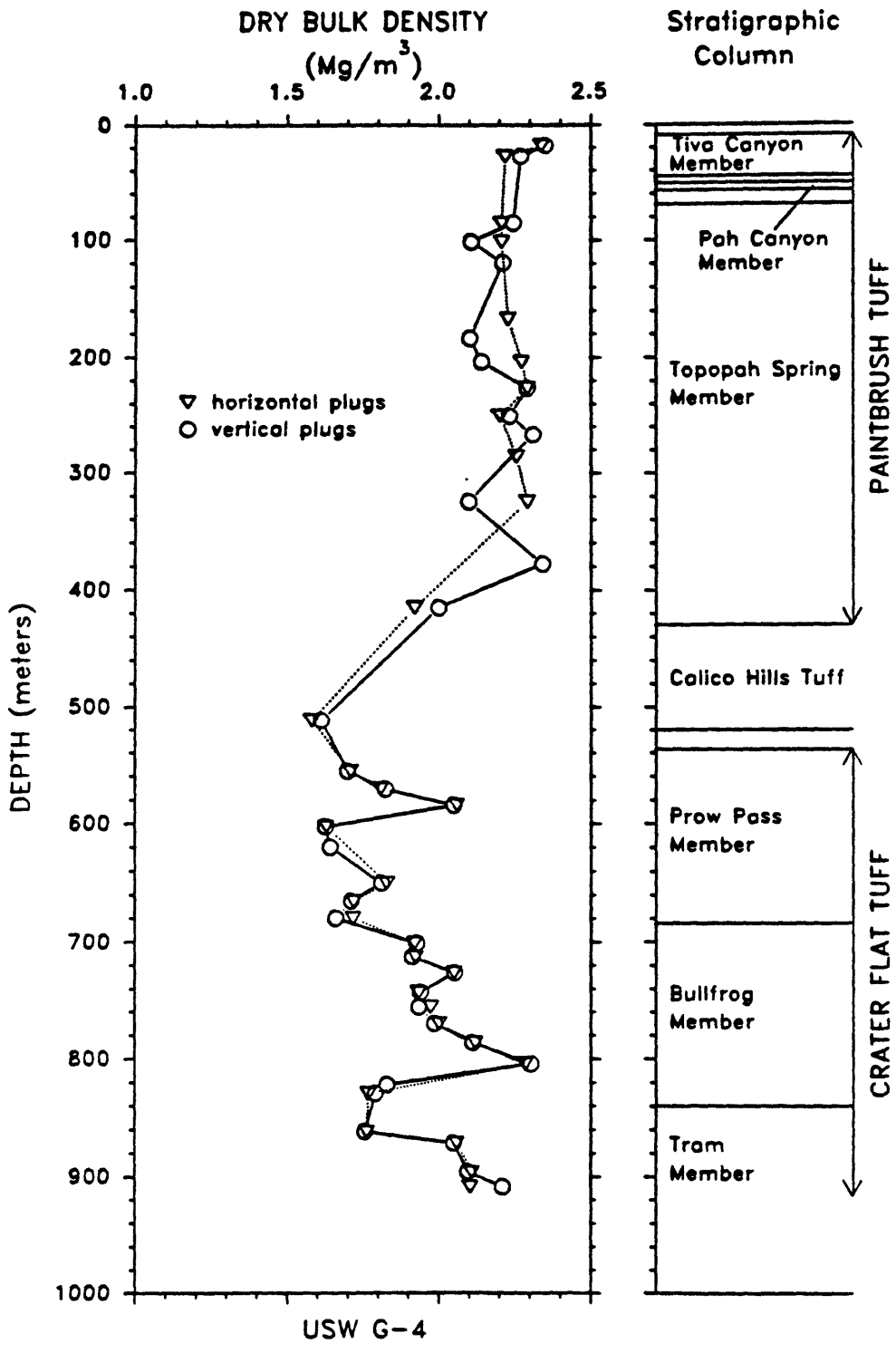

Figure 7. Dry bulk density values for USW G-4 horizontally and vertically oriented samples plotted as a function of sampling depth. The unlabeled intervals in the stratigraphic column are bedded ash-fall tuffs (Spengler and Chornack, 1984).

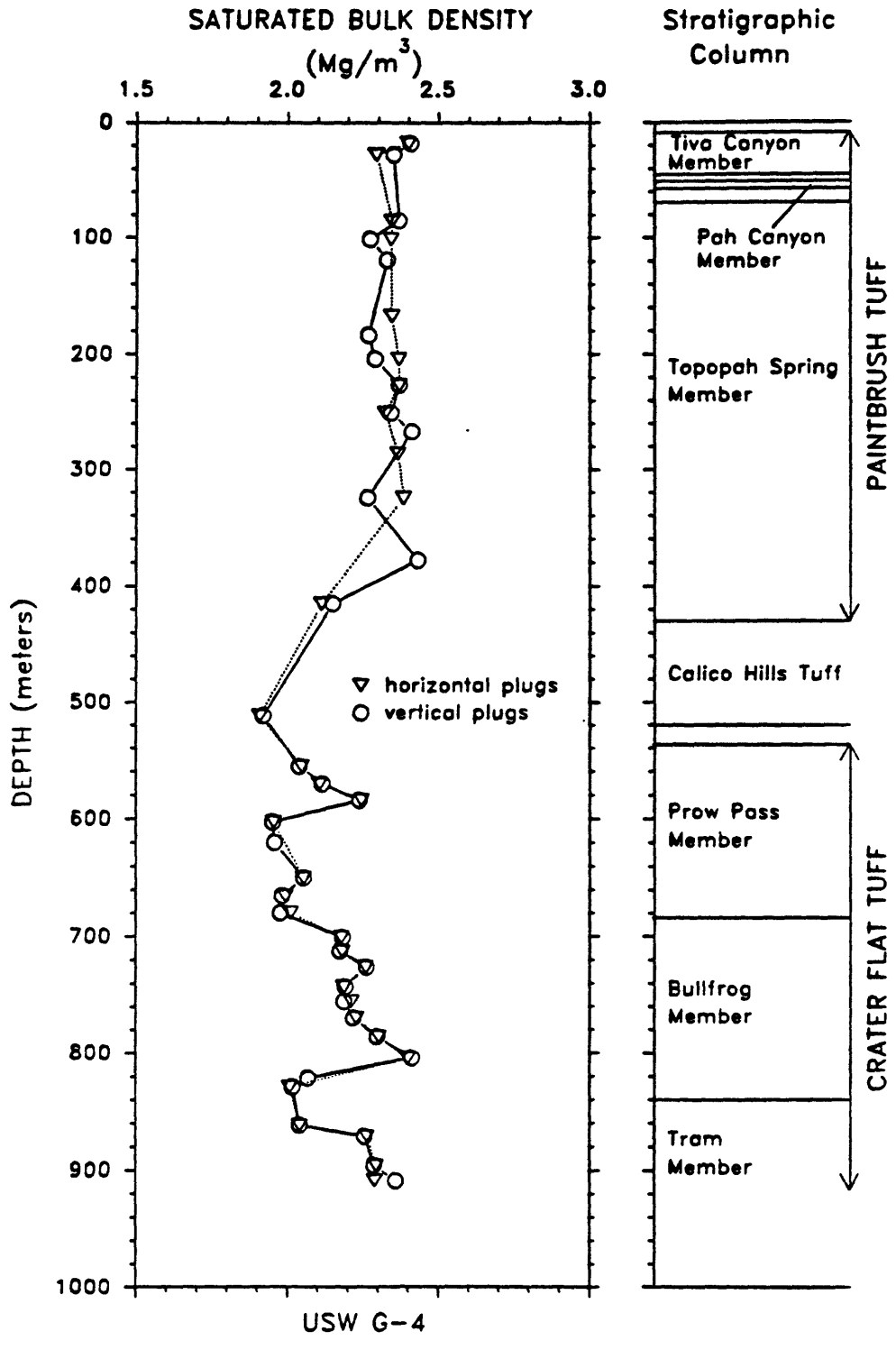

Figure 8. Saturated bulk density values for USW G-4 horizontally and vertically oriented samples plotted as a function of sampling depth. The unlabeled intervals in the stratigraphic column are bedded ash-fall tuffs (Spengler and Chornack, 1984).

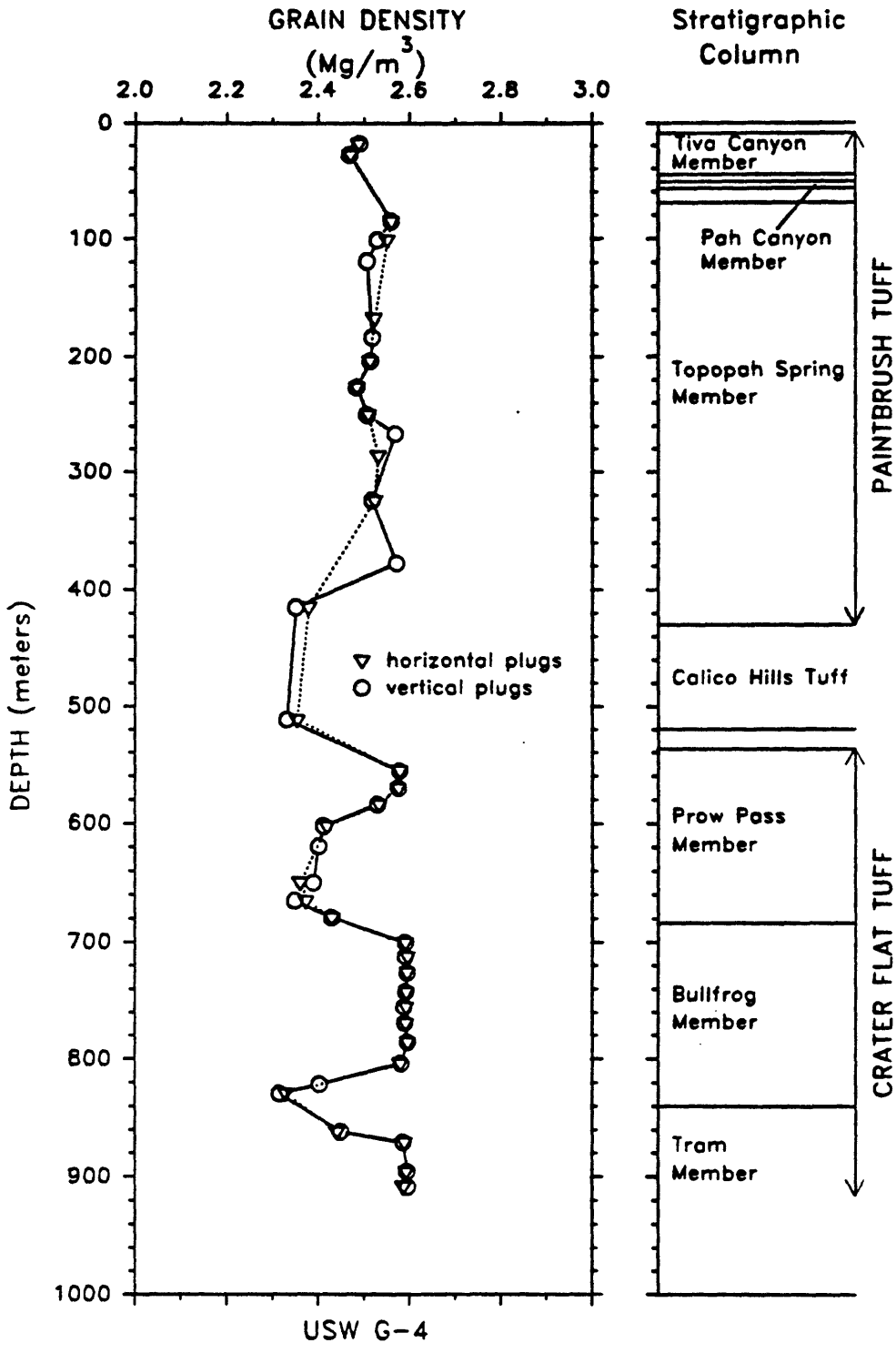

Figure 9. Grain density values for USW G-4 horizontally and vertically oriented samples plotted as a function of sampling depth. The unlabeled intervals in the stratigraphic column are bedded ash-fall tuffs (Spengler and Chornack, 1984).

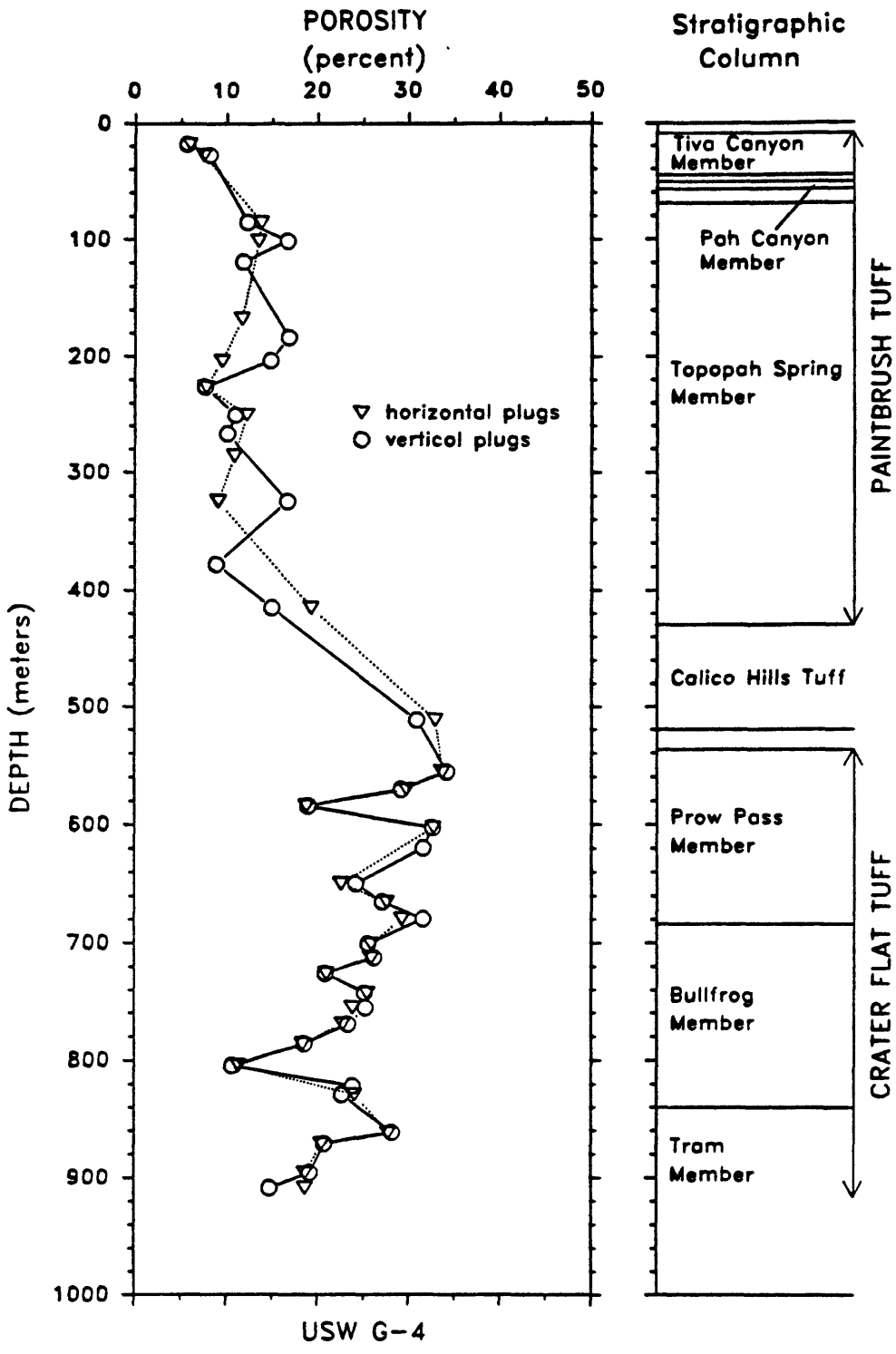

Figure 10. Porosity values for USW G-4 horizontally and vertically oriented samples plotted as a function of sampling depth. The unlabeled intervals in the stratigraphic column are bedded ash-fall tuffs (Spengler and Chornack, 1984).

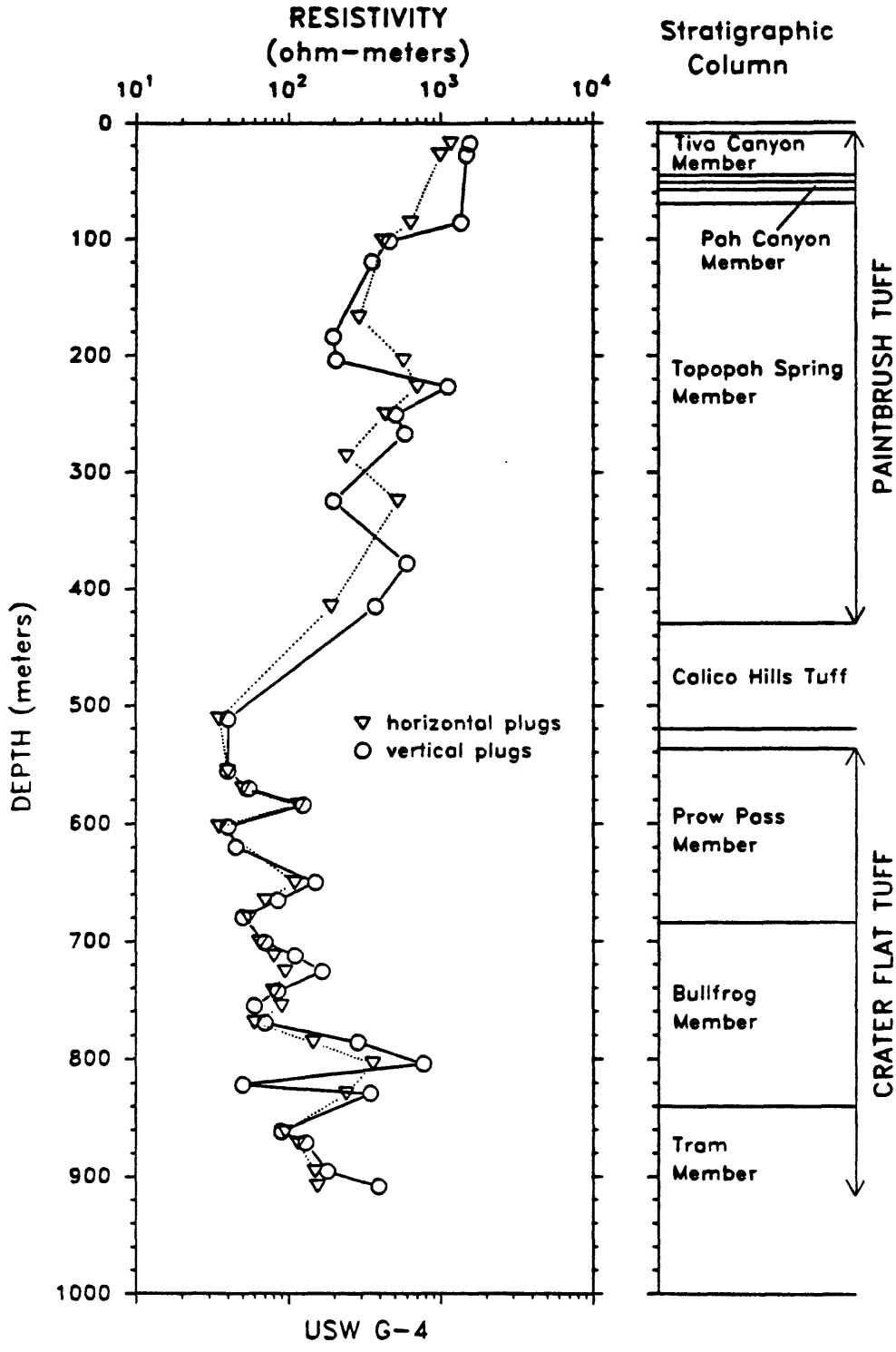

Figure 11. Resistivity values for USW G-4 horizontally and vertically oriented samples plotted as a function of sampling depth. The unlabeled intervals in the stratigraphic column are bedded ash-fall tuffs (Spengler and Chornack, 1984).

principal reason for the preponderance of lower resistivities in the horizontal plane. Microfractures may also affect the anisotropy in resistivity.

Permeability Measurements

Water permeabilities of the available samples were measured using the holding cell shown in figure 12. The enclosing or confining pressure was nominally maintained at 100 psi while distilled water under a driving pressure of 50 psi was forced through the sample along the line of its principal axis. Water flow was permitted to reach equilibrium before a series of readings were made to determine the effect of flow duration on permeability. The flow rate of a fixed volume of water (V) through a 1.6 mm diameter capillary was timed (t) and permeability (k) calculated from the equation

$$k = \mu V1/t\Delta PA,$$

where μ is the viscosity of the pore fluid in pascal-sec; ΔP is the net pressure difference across the length of the sample in pascals; and A and 1 are the cross-sectional area and length of the sample, respectively. Units of the permeability equation are in cm^2 but expressed in darcies by use of the conversion 1 darcy = 0.981 * 10^{-8} cm^2 (Olsen and Daniel, 1981).

Figure 13 shows the rather rapid decrease in permeability with respect to flow time observed for most nonfractured moderately to densely welded tuffs. The data were obtained using the horizontal plug taken from the USW GU-3 355.5 m depth core sample. The open-circle plot is the initial set of measurements which demonstrate a steep decline in permeability for the first hour and half of water flow. Permeability continued to decrease for the next three hours at a much slower rate. Water flow direction was then reversed and a few measurements taken over a period of about one and three-quarter hours. The first reading was approximately the same as determined from the initial series of measurements but the rate of decline was greater.

The decrease in permeability with time is believed to be caused by the redistribution of clay-sized particles clinging to the pore walls. These particles move so as to effectively close or restrict water migration through the capillaries connecting the pore spaces of the rock. The second series of measurements, obtained during flow reversal, demonstrated a more rapid decline in permeability with time suggesting that particulate matter, loosely attached to the pore walls, had been dislodged either by mechanical or leaching processes. According to Olsen and Daniel, 1981, leaching may increase particle mobility either because of expansion of diffuse double layers or because of removal of cements holding the particles to the pore walls.

To determine the effect a permeant other than distilled water has on permeability with respect to time, the sample was dried and resaturated with water collected from the J-13 water well located in Jackass Flats, approximately 6.2 km east of the G-3 borehole (figure 1). In the expectation that J-13 water would be similar in chemical composition to the original pore waters, the plot marked by the triangles was obtained. The curve essentially follows the reversed flow plot in the early stages and appears to indicate a greater decline in permeability with time than the measurements made with distilled water. The permeability of a rock in chemical balance with its pore water would show no change with time unless particles within the pore spaces were free to move.

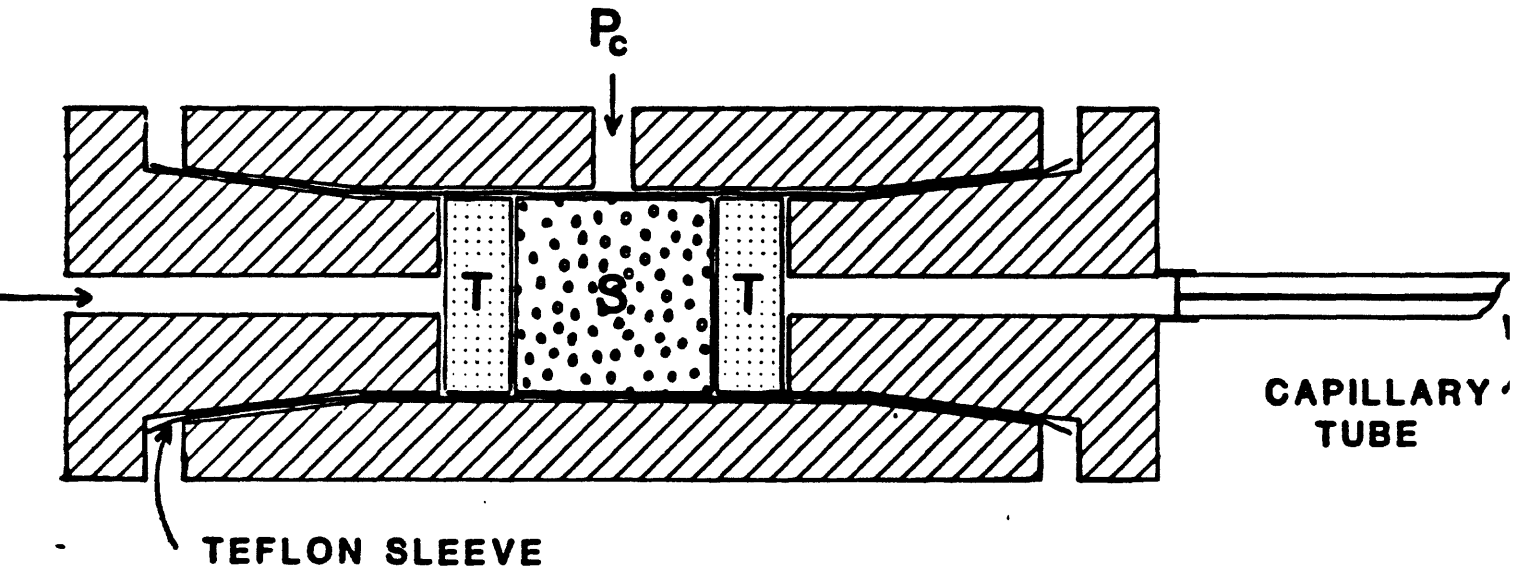

Figure 12. Diagram of the stainless steel sample holder used for permeability measurements. Porous teflon spacers, T, are designed to direct water flow uniformly through the sample, S, under confining pressure, Pc, and driving pressure, Pd, of 100 and 50 psi, respectively. The capillary tube is used to measure the rate of water flow through the rock.

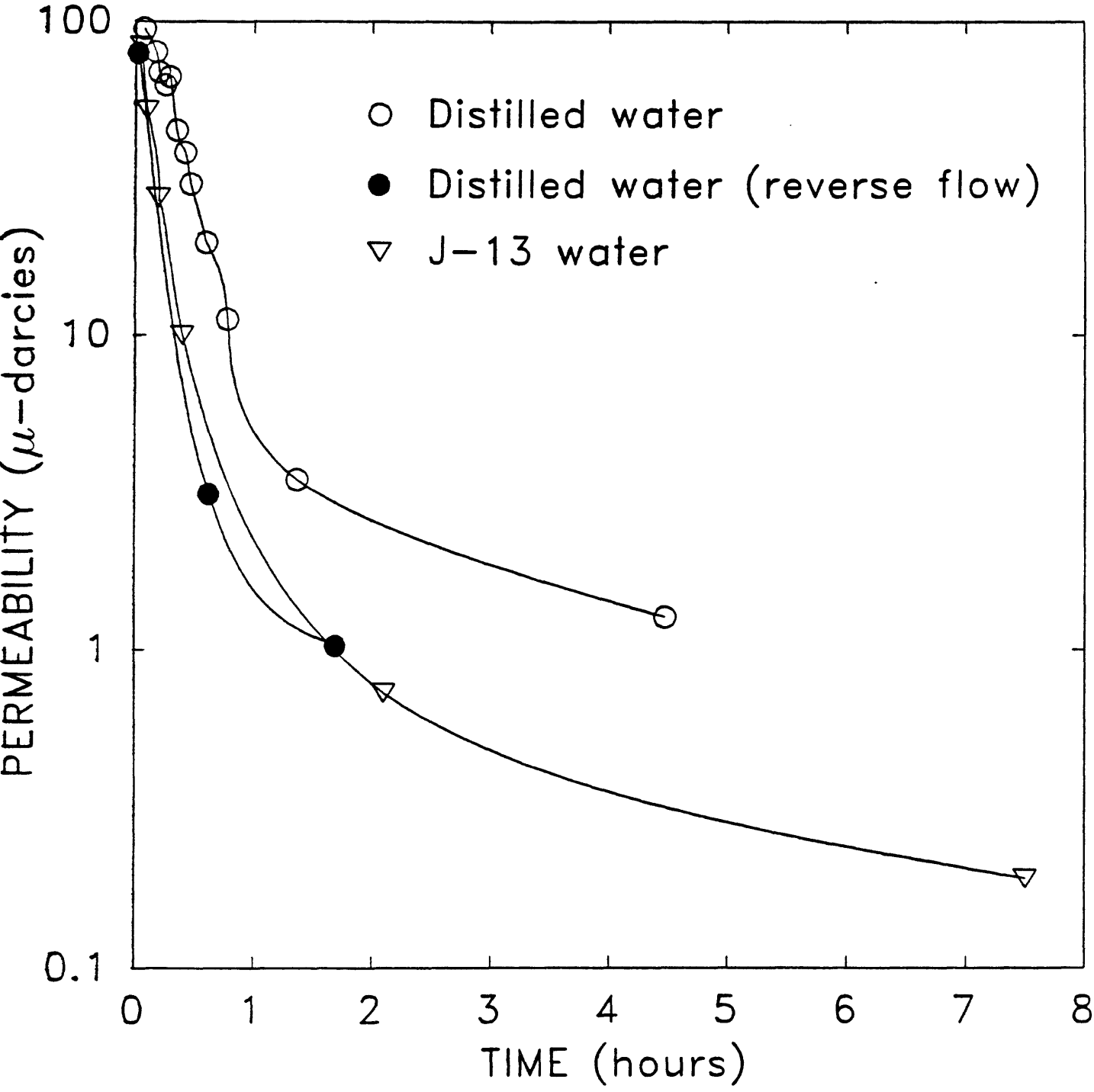

Figure 13. Plot demonstrating a decrease in permeability with time for the USW GU-3 sample from the 355.3 m depth. The initial run, shown by open circles, was made with distilled water as the permeant. The closed circles represent measurements made with a reversed water flow. Water from the Nevada Test Site J-13 water well produced the series of permeability values denoted by triangles.

The conclusion drawn from the three sets of measurements is that the initial permeabilities are reproducible despite differences in flow direction and in the chemical character of the permeants used. In each instance the permeability decreases with time at a rate dictated by the number of mobile particles within the pore spaces. It seems apparent that the longer water is forced through the rock the more particles become dislodged thereby constituting an increased impediment to water movement through the rock. Possibly this particular sample would become totally impervious to water migration with time as was noted for several other samples measured.

The permeabilities measured for the G-3 and G-4 borehole samples are listed in the Appendix as Tables 5 and 6, respectively. Where one value is shown only one measurement was taken. It was normally the practice to repeat the measurement on each sample up to the time when only small changes in permeability were noted. The second value listed in the tables is the final permeability determination. For some samples the decrease in permeability with time was negligible, whereas, in other instances, the decrease exceeded two orders of magnitude. The non-to-poorly welded samples generally demonstrated the smallest decline in permeability with time as a result of its higher porosity and possibly its larger internal pore dimensions. The moderate-to-densely welded tuff samples were most affected by particle movement within the pore spaces although some low permeability samples maintained essentially the same value throughout the entire measurement period.

The maximum or initial permeability values determined for the G-3 and G-4 samples have been plotted in figures 14 and 15, respectively. For plotting purposes, permeability values less than 1 microdarcy were assigned a value of 1 microdarcy. As indicated in figure 14, a wide range of permeabilities exist between sample pairs, within the individual tuff members, and between the various stratigraphic units. Where a core sample is represented by pairs, the horizontally aligned plugs generally had higher permeabilities, but many exceptions to this observation can be noted. Some of the larger discrepancies in permeability between sample pairs are believed to be caused by the occurrence of an unequal orientation or distribution of microfractures. The smaller differences in sample pair permeabilities are possibly the result of differences in the tortuosity of the flow path through the rock matrix.

The G-4 sample permeability values in figure 15 are similar to those shown in figure 14. A great deal of scatter is evident, particularly in the Paintbrush Tuff Members. As with the G-3 samples, the permeabilities of the horizontally aligned plugs are more often higher than those determined for the vertically aligned plugs. The Paintbrush Tuff samples are usually associated with the densely welded tuffs in which the pore dimensions are extremely small. With few exceptions the permeabilities of the sample pairs from within the 555 to 770 m interval of the Crater Flat Tuff are in much better agreement. In that same interval there are several examples of vertical sample permeability exceeding that of the horizontal sample. Below the 770 m depth all horizontal sample permeabilities exceed those of their vertical counterparts.

Two sample pairs from the USW GU-3 borehole, having virtually the same textural and compositional properties but differing somewhat in their permeabilities, were subjected to pore diameter measurements through the use of a mercury porosimeter. The instrument, a Micrometrics Model 9010, having the capability of invading pore diameters as small as 0.006 microns, forces

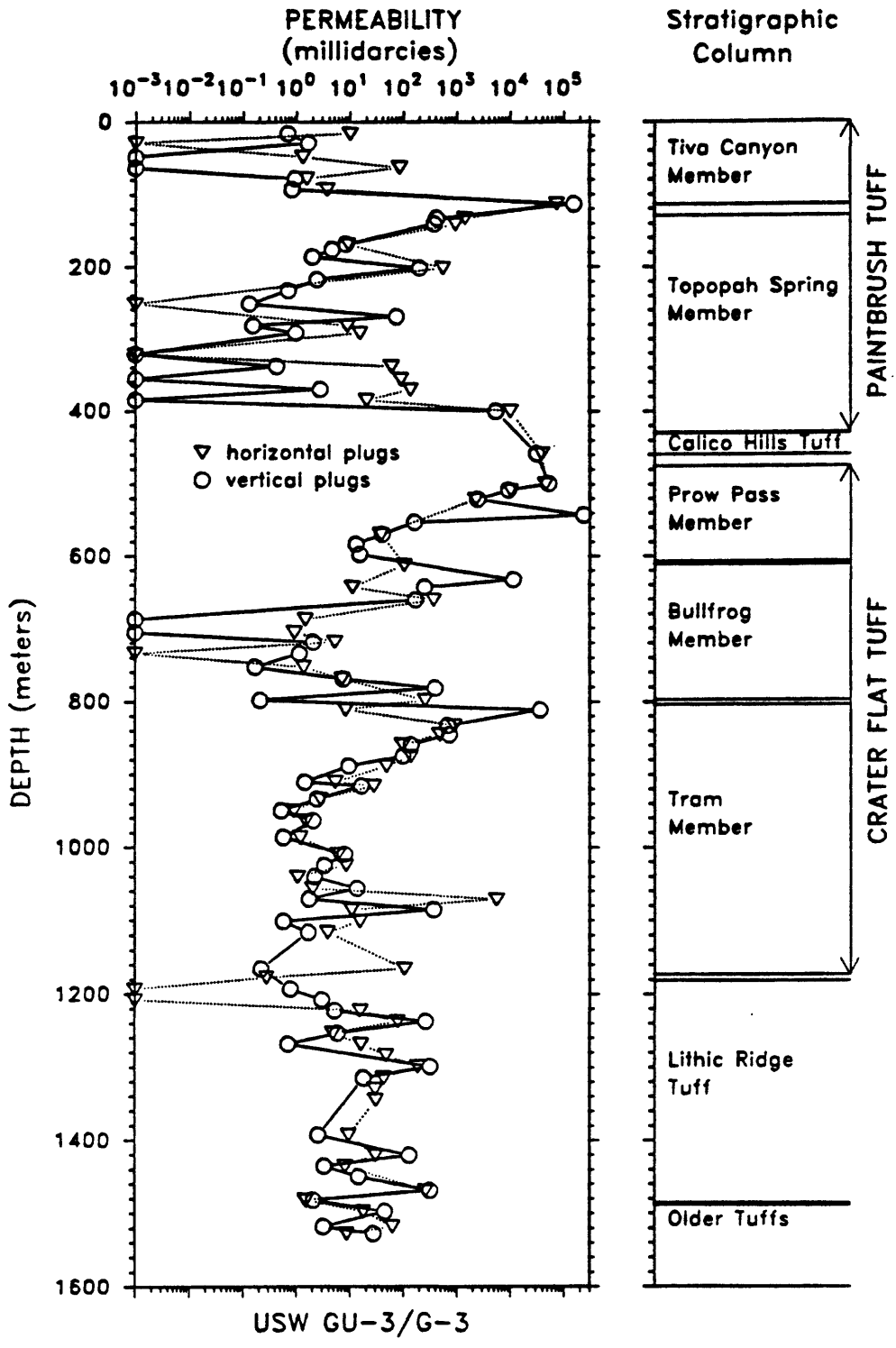

Figure 14. Initial (maximum) permeability values for USW GU-3/G-3 horizontally and vertically oriented samples plotted as a function of sampling depth. The unlabeled intervals in the stratigraphic column are bedded ash-fall tuffs (Scott and Castellanos, 1984).

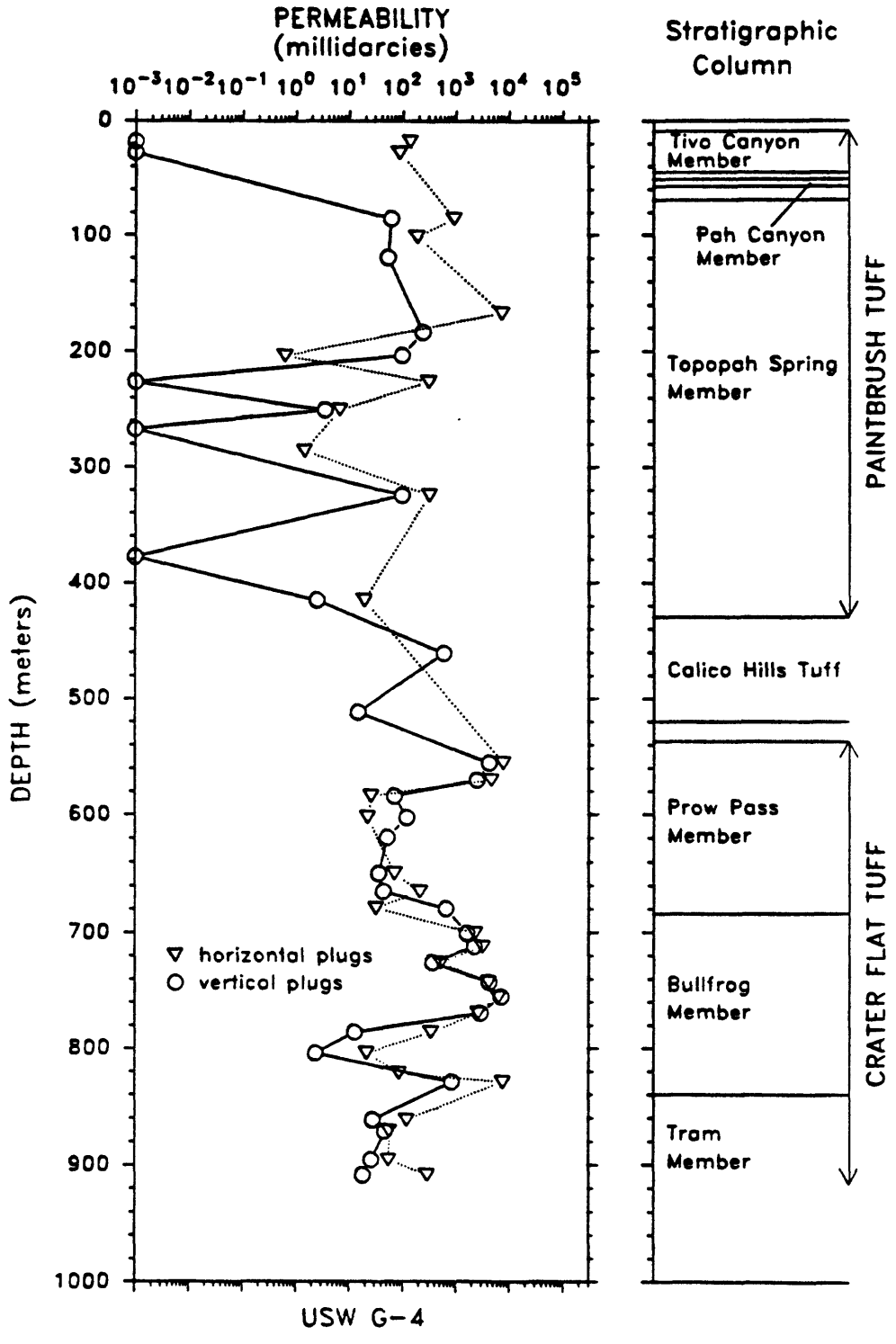

Figure 15. Initial (maximum) permeability values for USW G-4 horizontally and vertically oriented samples plotted as a function of sampling depth. The unlabeled intervals in the stratigraphic column are bedded ash-fall tuffs (Spengler and Chornack, 1984).

mercury into the pore spaces of a rock at sequentially stepped pressures up to a maximum of 30,000 psi. The instrument is computer controlled and, as part of the analysis, produces printouts of data as shown in figures 16 and 17. A general description of the operating principles of a mercury porosimeter has been provided by Johnson (1979).

Figure 16 illustrates the pore diameter distribution within samples taken from the 355.5 m depth (Topopah Springs Member of the Paintbrush Tuff) as a percentage of the total porosity of the rock. With minor variations, the plots are essentially the same depicting tightly clustered pore diameters averaging 0.025 microns for each sample. Very few pore structures within the samples exceed diameters of 0.1 microns. Despite the striking similarity in pore dimension, porosity, and in the mineral content as implied by the grain density of the samples, the vertically aligned plug is impermeable (less than 0.01 microdarcies) whereas the horizontally oriented plug was determined to have a permeability of 95 microdarcies. In the vertical mode the flow paths are obviously discontinuous, but horizontally the pore spaces are sufficiently interconnected so as to facilitate water transport. The indicated resistivities on figure 16 are also indicative of a more accommodating flow path for electrical current as well as fluid.

Figure 17 is a pore diameter distribution plot of Topopah Spring samples from the 140.6 m depth which supports the inference made based on the data shown in figure 16. The pore diameter distribution in each plug is virtually identical as are the other listed properties except for permeability and resistivity. Average pore diameter for each plug is 0.091 microns indicating that the samples are less welded than those from the 355.5 m depth interval, and, as a consequence, have higher permeabilities. In view of the range of permeabilities determined for the total number of samples measured, the permeability contrast between the 140.6 m plugs is of minor significance. However, the higher permeability and lower resistivity determined for the horizontal plug suggests that the continuity and possibly the tortuosity of the flow paths within the rock matrix is a major factor in controlling the permeability of the welded tuffs.

SUMMARY

Two hundred and twenty six plugs, 2.54 cm in length and diameter, were drilled from core samples obtained from the Yucca Mountain USW GU-3/G-3 and USW G-4 boreholes located adjacent to the southwest boundary of the Nevada Test Site, Nye County, Nevada. Of these, two hundred were paired samples drilled from the original core in an axial and perpendicular orientation. The core was selected at the drill site so as to be representative of the major lithologic variations observed within each stratigraphic unit. Borehole G-3, drilled to a depth of 1533.8 meters, intersected the Tiva Canyon and Topopah Spring Members of the Paintbrush Tuff; the Calico Hills Tuff; the Prow Pass, Bullfrog, and Tram Members of the Crater Flat Tuff; Lithic Ridge Tuff; and Older Tuffs. Borehole G-4, 914.7 meters deep, penetrated only to within the Tram Member of the Crater Flat Tuff.

With few exceptions, the grain density data indicates a uniform mineral content between the paired samples. The pattern of variation shown on the bulk density plots closely follows the inverse of porosity demonstrating a dependence upon textural rather than compositional changes within the rock. Low porosities are associated with welded and silicified tuffs whereas the higher porosities indicate intervals of non-welded tuffs.

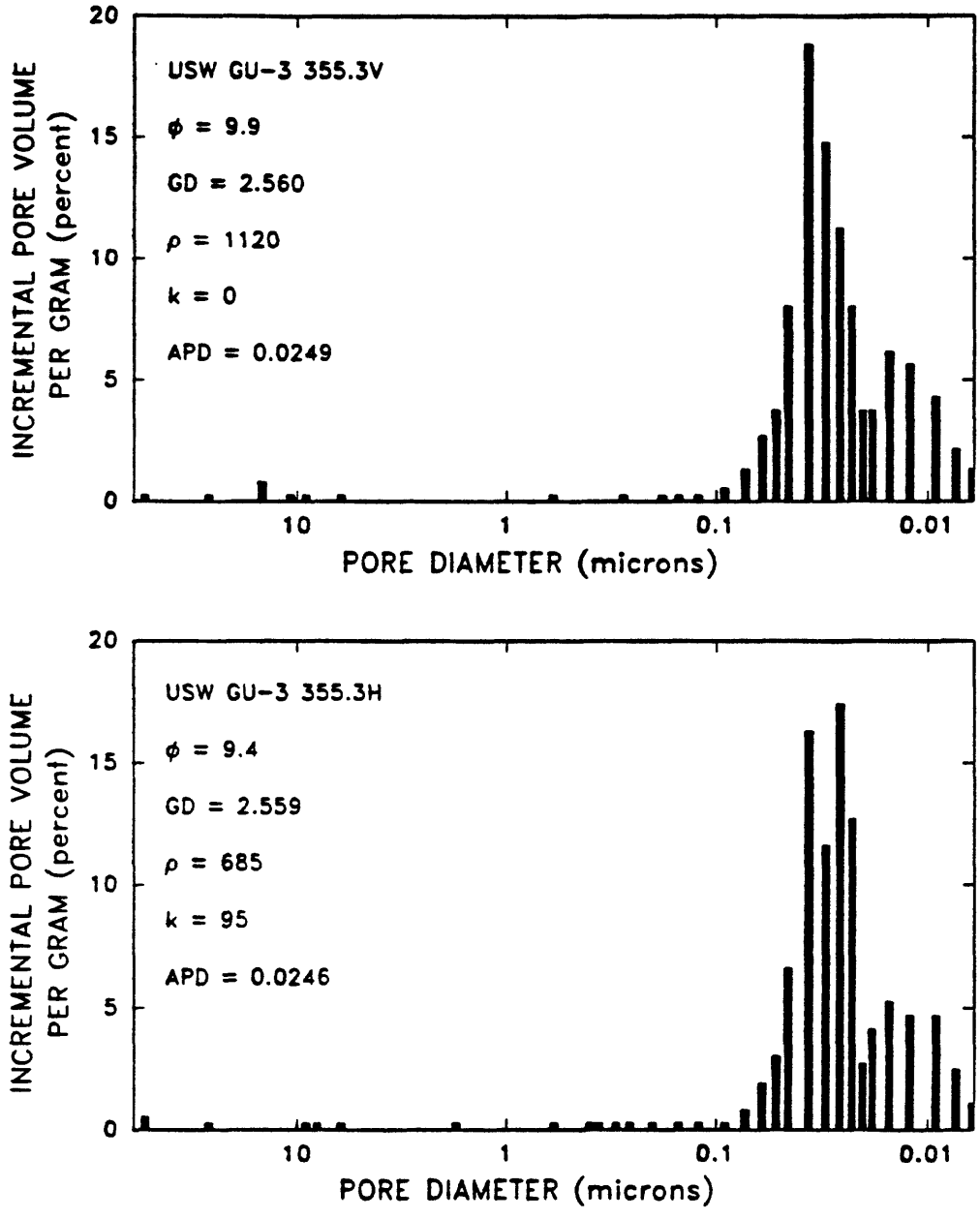

Figure 16. Pore diameter distribution determined for the vertical (top) and horizontal (bottom) plugs obtained from the USW GU-3 355.3 m core sample. Property values listed for each sample are porosity, ϕ, in percent; grain density, GD, in Mg/m^3; resistivity, ρ, in ohm-m; permeability, k, in microdarcies; and average pore dimension, APD, in microns.

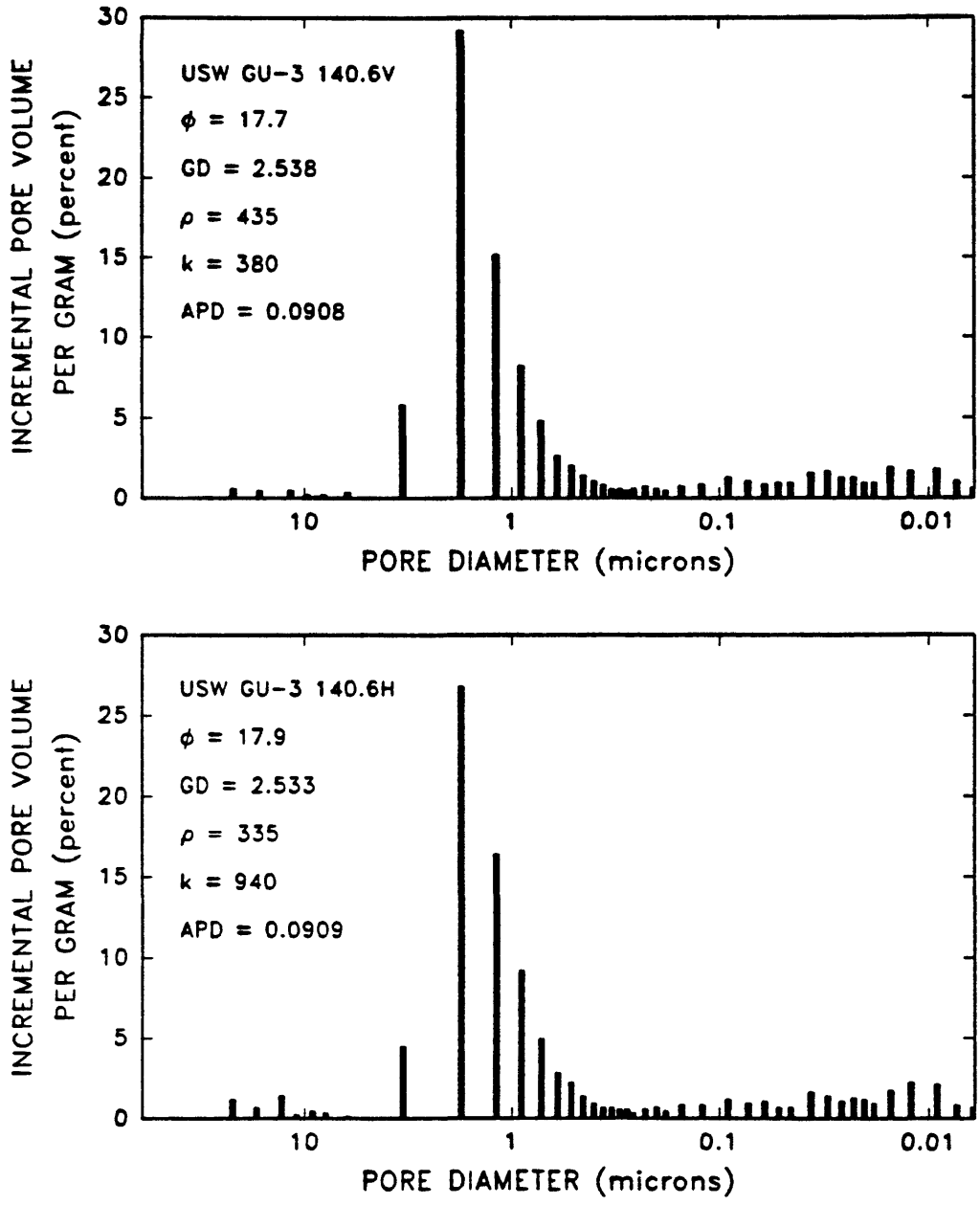

Figure 17. Pore diameter distribution determined for the vertical (top) and horizontal (bottom) plugs obtained from the USW GU-3 140.6 m core sample. Property values listed for each sample are porosity, ϕ, in percent; grain density, GD, in Mg/m^3; resistivity, ρ, in ohm-m; permeability, k, in microdarcies; and average pore dimension, APD, in microns.

Two sample pairs were examined for their pore size distribution expressed as a percent fraction of the total pore volume. The higher porosity pair had the higher permeabilities as expected in rocks free of clays, zeolites, and microfractures. The horizontal and vertical components of each pair had virtually the same porosity and pore dimensions but differed in permeability and resistivity indicating the importance of pore continuity in controlling both water and current flow through the rock. Sowers, 1981, states that if the rock particles are elongated and oriented, the pores will be directional and the permeability anisotropic. In welded tuff it might be anticipated that the welding process would cause a particle alignment in the horizontal plane which was normally the circumstance experienced. However, exceptions were encountered for which there is no ready explanation.

Of the 67 G-3 sample pairs measured, 39 demonstrated a correspondence of lower resistivity and higher permeability in the horizontally oriented samples. Only seven of the sample pairs showed a similar correspondence amongst the vertically oriented samples. Nineteen sample pairs indicated no correspondence between resistivity and permeability suggesting current flow within the samples occurs by means of surface conduction rather than by ionic conduction through the pore waters. Two sample pairs proved to be equal in resistivity and permeability in both the vertical and horizontal directions.

Similarly, of the 28 sample pairs taken from the G-4 borehole, the lower resistivity and higher permeability correspondence occurs in 20 of the horizontally aligned samples, 3 in the vertically oriented samples, and 5 show no correlation. Clearly, the resistivities are typically lower and the permeabilities higher in the horizontally oriented samples confirming a pore alignment more conducive to current and water flow than that found in the vertically oriented samples. Although the ash-flow tuffs are not considered to take on a bedding aspect during their formation, there is apparently a tendency to develop an interconnected pore structure of greater continuity or lower tortuosity along the horizontal plane of the rock layers.

Appendix: Tables of Rock Property Values

Table 1. Density values obtained on vertically and horizontally oriented core samples from the USW GU-3/G-3 borehole: Leader (-) indicates sample was not suitable for measurement.

Sample depth in meters (feet)		Dry Bulk Density ---Mg/m^3---		Saturated Bulk Density ---Mg/m^3---		Grain Density ---Mg/m^3---	
		Vert.	Hor.	Vert.	Hor.	Vert.	Hor.
16.6	(54.2)	2.266	2.192	2.355	2.311	2.487	2.489
29.4	(96.3)	2.192	2.181	2.309	2.300	2.483	2.475
48.4	(158.8)	2.295	2.305	2.371	2.378	2.484	2.487
63.3	(207.5)	2.307	2.303	2.378	2.375	2.482	2.481
78.4	(257.0)	2.303	2.308	2.378	2.383	2.489	2.495
93.2	(305.7)	2.250	2.289	2.343	2.364	2.480	2.476
113.1	(370.9)	(-)	1.392	(-)	1.801	(-)	2.355
132.7	(435.2)	2.125	2.122	2.295	2.292	2.561	2.557
140.6	(461.1)	2.088	2.079	2.265	2.258	2.538	2.533
168.4	(552.3)	2.138	2.131	2.276	2.272	2.482	2.480
175.6	(576.0)	2.186	(-)	2.305	(-)	2.481	(-)
186.1	(610.3)	2.196	2.143	2.305	2.277	2.465	2.476
201.3	(660.3)	2.141	2.144	2.351	2.284	2.709	2.493
217.6	(713.8)	2.279	(-)	2.366	(-)	2.496	(-)
233.2	(765.0)	2.153	(-)	2.285	(-)	2.479	(-)
251.7	(825.6)	2.325	2.326	2.391	2.392	2.490	2.490
269.5	(884.1)	2.304	(-)	2.411	(-)	2.579	(-)
282.0	(925.0)	2.276	2.268	2.372	2.363	2.518	2.506
292.0	(957.7)	2.300	2.290	2.387	2.386	2.520	2.532
321.9	(1055.8)	2.321	2.325	2.423	2.476	2.584	2.587
338.1	(1108.9)	2.339	2.325	2.427	2.411	2.564	2.544
355.5	(1165.9)	2.307	2.318	2.406	2.412	2.560	2.559
369.9	(1213.2)	2.314	2.318	2.340	2.341	2.377	2.372
384.7	(1261.8)	2.299	2.295	2.329	2.326	2.370	2.370
399.7	(1310.9)	1.689	1.649	1.962	1.936	2.322	2.313
457.9	(1501.8)	1.463	1.439	1.809	1.797	2.238	2.240
499.3	(1637.7)	(-)	1.643	(-)	1.997	(-)	2.545
508.1	(1666.7)	1.737	1.725	2.054	2.047	2.544	2.544
520.3	(1706.6)	1.870	1.871	2.132	2.133	2.535	2.537
552.9	(1813.5)	1.451	(-)	1.838	(-)	2.368	(-)
569.2	(1866.9)	1.587	1.724	1.916	1.995	2.363	2.366
583.1	(1912.7)	1.595	(-)	1.920	(-)	2.364	(-)
597.1	(1958.4)	1.543	(-)	1.887	(-)	2.352	(-)
612.3	(2008.4)	(-)	1.605	(-)	1.930	(-)	2.378
632.6	(2075.0)	1.798	(-)	2.097	(-)	2.564	(-)
643.3	(2110.0)	2.217	2.219	2.351	2.352	2.561	2.559
660.8	(2167.5)	2.089	2.097	2.270	2.276	2.549	2.553
672.2	(2204.9)	2.315	2.321	2.405	2.408	2.544	2.542
688.0	(2256.8)	2.332	2.332	2.417	2.419	2.549	2.552
705.8	(2315.0)	(-)	2.352	(-)	2.432	(-)	2.556
718.5	(2356.7)	2.379	2.383	2.449	2.452	2.559	2.559
733.9	(2407.2)	2.361	2.365	2.433	2.437	2.544	2.547
752.6	(2468.5)	2.448	2.428	2.503	2.489	2.590	2.585
768.8	(2521.5)	2.261	2.283	2.367	2.380	2.529	2.527
781.2	(2562.4)	1.622	(-)	1.941	(-)	2.383	(-)
798.0	(2617.5)	1.901	(-)	2.125	(-)	2.449	(-)

Table 1 (continued)

811.1	(2660.5)	1.915	1.608	2.127	1.938	2.431	2.401
832.6	(2730.9)	1.752	1.774	2.063	2.077	2.543	2.543
845.0	(2771.7)	1.858	1.876	2.132	2.144	2.562	2.562
859.1	(2817.7)	1.887	1.890	2.148	2.150	2.553	2.556
874.5	(2868.2)	1.941	1.956	2.181	2.191	2.555	2.559
888.3	(2913.6)	2.098	2.072	2.282	2.270	2.572	2.583
910.4	(2986.1)	2.191	2.160	2.347	2.328	2.596	2.596
915.9	(3004.1)	2.203	2.250	2.348	2.384	2.577	2.596
933.5	(3062.0)	2.233	2.228	2.369	2.365	2.584	2.583
949.8	(3115.4)	2.210	2.193	2.336	2.325	2.528	2.527
963.3	(3159.6)	2.090	2.067	2.255	2.241	2.502	2.503
986.3	(3235.0)	2.392	2.387	2.454	2.447	2.550	2.539
1009.4	(3310.7)	1.860	1.933	2.121	2.173	2.516	2.542
1024.5	(3360.3)	1.955	1.985	2.181	2.204	2.528	2.541
1040.0	(3411.2)	1.930	1.953	2.160	2.179	2.506	2.524
1056.1	(3463.9)	1.917	1.890	2.143	2.124	2.477	2.466
1070.5	(3511.2)	1.942	1.995	2.160	2.200	2.482	2.510
1085.4	(3560.2)	1.981	2.025	2.194	2.224	2.516	2.528
1101.0	(3611.3)	2.041	2.088	2.219	2.251	2.484	2.494
1115.6	(3659.3)	2.057	2.092	2.225	2.255	2.473	2.500
1165.5	(3822.7)	2.335	2.097	2.437	2.296	2.601	2.617
1177.2	(3861.2)	(-)	2.096	(-)	2.258	(-)	2.502
1192.8	(3912.3)	1.891	2.004	2.148	2.216	2.545	2.544
1207.5	(3960.5)	1.882	2.087	2.141	2.259	2.541	2.521
1222.2	(4008.9)	1.921	1.924	2.160	2.176	2.523	2.572
1237.4	(4058.7)	1.900	1.802	2.135	2.076	2.483	2.482
1253.2	(4110.6)	1.988	2.043	2.197	2.228	2.513	2.508
1268.0	(4159.0)	1.978	1.992	2.201	2.210	2.545	2.546
1283.4	(4209.5)	(-)	2.062	(-)	2.250	(-)	2.538
1299.1	(4261.0)	1.935	1.920	2.161	2.158	2.498	2.520
1314.6	(4311.8)	2.002	1.999	2.214	2.220	2.543	2.567
1329.6	(4361.0)	2.099	2.092	2.298	2.297	2.621	2.631
1344.5	(4409.9)	(-)	1.996	(-)	2.213	(-)	2.548
1392.6	(4567.8)	2.100	2.186	2.288	2.338	2.585	2.577
1420.7	(4659.9)	2.075	2.137	2.264	2.301	2.558	2.555
1435.3	(4707.9)	2.134	2.182	2.306	2.338	2.577	2.584
1450.0	(4755.9)	2.024	(-)	2.233	(-)	2.559	(-)
1469.1	(4818.6)	2.001	2.036	2.207	2.226	2.521	2.513
1482.0	(4860.8)	2.027	2.066	2.225	2.247	2.528	2.523
1497.2	(4910.7)	2.088	2.102	2.242	2.247	2.469	2.460
1517.7	(4977.9)	2.086	2.066	2.276	2.259	2.574	2.560
1527.4	(5009.8)	2.328	2.107	2.403	2.273	2.516	2.526

Table 2. Resistivity and porosity values obtained on vertically and horizontally oriented core samples from the USW GU-3/G-3 borehole. Leader (-) indicates sample was not suitable for measurement.

Sample depth in meters (feet)	Resistivity (ohm- meters)		Porosity (percent)	
	Vert.	Hor.	Vert.	Hor.
16.6 (54.2)	5780	2100	8.9	11.9
29.4 (96.3)	2340	1810	11.7	11.9
48.4 (158.8)	4840	4660	7.6	7.3
63.3 (207.5)	4240	1600	7.0	7.2
78.4 (257.0)	2910	2090	7.5	7.5
93.2 (305.7)	1270	1240	9.3	7.5
113.1 (370.9)	(-)	25	(-)	40.9
132.7 (435.2)	465	310	17.0	17.0
140.6 (461.1)	435	335	17.7	17.9
168.4 (552.3)	610	260	13.9	14.1
175.6 (576.0)	615	(-)	11.9	(-)
186.1 (610.3)	700	350	10.9	13.4
201.3 (660.3)	105	270	20.9	14.0
217.6 (713.8)	795	(-)	8.7	(-)
233.2 (765.0)	520	(-)	13.1	(-)
251.7 (825.6)	1060	1415	6.6	6.6
269.5 (884.1)	410	(-)	10.7	(-)
282.0 (925.0)	510	520	9.6	9.5
292.0 (957.7)	430	400	8.7	9.6
321.9 (1055.8)	3690	1080	10.2	10.1
338.1 (1108.9)	1320	715	8.8	8.6
355.5 (1165.9)	1120	685	9.9	9.4
369.9 (1213.2)	790	415	2.6	2.2
384.7 (1261.8)	2280	975	3.0	3.2
399.7 (1310.9)	115	95	27.3	28.7
457.9 (1501.8)	55	55	34.6	35.7
499.3 (1637.7)	(-)	40	(-)	35.4
508.1 (1666.7)	75	65	31.7	32.2
520.3 (1706.6)	115	105	26.2	26.3
552.9 (1813.5)	60	(-)	38.7	(-)
569.2 (1866.9)	55	50	32.8	27.1
583.1 (1912.7)	45	(-)	32.5	(-)
597.1 (1958.4)	50	(-)	34.4	(-)
612.3 (2008.4)	(-)	30	(-)	32.5
632.6 (2075.0)	95	(-)	29.9	(-)
643.3 (2110.2)	330	300	13.5	13.3
660.8 (2167.5)	150	125	18.0	17.8
672.2 (2204.9)	435	360	9.0	8.7
688.0 (2256.8)	595	510	8.5	8.6
705.8 (2315.0)	(-)	735	(-)	8.0
718.5 (2356.7)	930	915	7.1	6.9
733.9 (2407.2)	700	545	7.2	7.1
752.6 (2468.5)	4200	1280	5.5	6.1
768.8 (2521.5)	460	490	10.6	9.6
781.2 (2562.4)	70	(-)	31.9	(-)
798.0 (2617.5)	45	(-)	22.4	(-)
811.1 (2660.5)	95	40	21.2	33.1
832.6 (2730.9)	65	60	31.1	30.2

Table 2 (continued)

845.0 (2771.7)	90	75	27.5	26.8
859.1 (2817.7)	90	70	26.1	26.0
874.5 (2868.2)	110	90	24.0	23.6
888.3 (2913.6)	165	90	18.4	19.8
910.4 (2986.1)	460	195	15.6	16.8
915.9 (3004.1)	425	315	14.5	13.3
933.5 (3062.0)	555	245	13.6	13.7
949.8 (3115.4)	350	225	12.6	13.2
963.3 (3159.6)	300	115	16.5	17.4
986.3 (3235.0)	1000	790	6.2	6.0
1009.4 (3310.7)	70	65	26.1	24.0
1024.5 (3360.3)	55	35	22.7	21.9
1040.0 (3411.2)	45	55	23.0	22.6
1056.1 (3463.9)	75	50	22.6	23.3
1070.5 (3511.2)	60	55	21.8	20.5
1085.4 (3560.2)	55	55	21.3	19.9
1101.0 (3611.3)	55	155	17.9	16.3
1115.6 (3659.3)	50	40	16.8	16.3
1165.5 (3822.7)	285	35	10.2	19.9
1177.2 (3861.2)	(-)	55	(-)	16.2
1192.8 (3912.3)	65	45	25.7	21.2
1207.5 (3960.5)	45	50	26.0	17.2
1222.2 (4008.9)	55	45	23.9	25.2
1237.4 (4058.7)	65	45	23.5	27.4
1253.2 (4110.6)	90	100	20.9	18.6
1268.0 (4159.0)	55	45	22.3	21.7
1283.4 (4209.5)	(-)	60	(-)	18.7
1299.1 (4261.0)	85	65	22.5	23.8
1314.6 (4311.8)	65	35	21.3	22.1
1329.6 (4361.0)	20	225	19.9	20.5
1344.5 (4409.9)	(-)	35	(-)	21.7
1392.6 (4567.8)	25	40	18.8	15.2
1420.7 (4659.9)	40	45	18.9	16.3
1435.3 (4707.9)	55	55	17.2	15.6
1450.0 (4755.9)	45	(-)	20.9	(-)
1469.1 (4818.6)	90	95	20.6	19.0
1482.0 (4860.8)	50	40	19.8	18.1
1497.2 (4910.7)	75	60	15.4	14.6
1517.7 (4977.9)	25	25	19.0	19.3
1527.4 (5009.8)	450	60	7.5	16.6

Table 3. Density values obtained on vertically and horizontally oriented core samples from the USW G-4 borehole. Leader (-) indicates sample was not suitable for measurement.

Sample depth in meters (feet)		Dry Bulk Density ---Mg/m^3---		Saturated Bulk Density ---Mg/m^3---		Grain Density ---Mg/m^3---	
		Vert.	Hor.	Vert.	Hor.	Vert.	Hor.
18.0	(59.0)	2.350	2.338	2.406	2.399	2.491	2.489
27.7	(90.8)	2.270	2.219	2.350	2.294	2.469	2.470
85.5	(280.4)	2.245	2.207	2.368	2.345	2.560	2.560
101.3	(332.3)	2.106	2.207	2.273	2.342	2.529	2.551
119.0	(390.3)	2.211	(-)	2.329	(-)	2.506	(-)
167.2	(548.4)	(-)	2.228	(-)	2.344	(-)	2.522
183.7	(602.6)	2.102	(-)	2.268	(-)	2.518	(-)
203.8	(668.6)	2.141	2.273	2.289	2.368	2.514	2.513
226.4	(742.5)	2.292	2.291	2.369	2.369	2.484	2.484
250.4	(821.2)	2.232	2.202	2.342	2.324	2.507	2.509
266.9	(875.5)	2.310	(-)	2.411	(-)	2.568	(-)
285.9	(937.6)	(-)	2.256	(-)	2.365	(-)	2.531
324.5	(1064.5)	2.098	2.292	2.265	2.384	2.518	2.523
377.8	(1239.2)	2.342	(-)	2.431	(-)	2.571	(-)
415.1	(1361.5)	1.999	1.643	2.149	1.944	2.351	2.348
511.7	(1678.4)	1.611	1.580	1.920	1.909	2.332	2.354
555.7	(1822.8)	1.698	1.709	2.039	2.047	2.579	2.579
570.3	(1870.7)	1.823	1.807	2.115	2.106	2.576	2.576
584.1	(1915.8)	2.049	2.058	2.239	2.245	2.530	2.533
602.4	(1976.0)	1.625	1.628	1.951	1.955	2.412	2.419
619.6	(2032.4)	1.641	(-)	1.958	(-)	2.401	(-)
649.8	(2131.2)	1.811	1.828	2.053	2.054	2.389	2.361
665.2	(2181.8)	1.712	1.719	1.983	1.994	2.349	2.373
679.4	(2228.5)	1.660	1.717	1.977	2.011	2.429	2.430
700.6	(2298.0)	1.926	1.920	2.183	2.179	2.591	2.591
712.4	(2336.8)	1.912	1.923	2.174	2.182	2.591	2.596
726.1	(2381.6)	2.052	2.050	2.261	2.260	2.595	2.595
742.7	(2436.1)	1.940	1.933	2.192	2.187	2.592	2.593
755.5	(2478.0)	1.934	1.973	2.187	2.212	2.588	2.593
769.4	(2523.7)	1.985	2.000	2.218	2.228	2.590	2.592
785.9	(2577.7)	2.112	2.120	2.298	2.303	2.596	2.596
804.1	(2637.5)	2.304	2.285	2.412	2.399	2.582	2.580
821.5	(2694.6)	1.829	(-)	2.068	(-)	2.403	(-)
829.1	(2719.5)	1.790	1.768	2.017	2.009	2.316	2.329
861.7	(2826.2)	1.758	1.763	2.041	2.041	2.450	2.442
871.0	(2856.8)	2.048	2.059	2.256	2.264	2.587	2.589
895.9	(2938.6)	2.096	2.109	2.288	2.295	2.595	2.593
908.5	(2979.8)	2.211	2.104	2.359	2.291	2.596	2.587

Table 4. Resistivity and porosity of vertically and horizontally oriented core samples obtained from the USW G-4 borehole. Leader (-) indicates sample was not suitable for measurement.

Sample depth in meters (feet)		Resistivity (ohm- meters)		Porosity (percent)	
		Vert.	Hor.	Vert.	Hor.
18.0	(59.0)	1560	1170	5.7	6.0
27.7	(90.8)	1480	990	8.1	7.5
85.5	(280.4)	1350	635	12.3	13.8
101.3	(332.3)	460	420	16.7	13.5
119.0	(390.3)	355	(-)	11.8	(-)
167.2	(548.4)	(-)	290	(-)	11.7
183.7	(602.6)	195	(-)	16.8	(-)
203.8	(668.6)	205	570	14.8	9.5
226.4	(742.5)	1110	700	7.7	7.8
250.4	(821.2)	505	435	11.0	12.2
266.9	(875.5)	580	(-)	10.1	(-)
285.9	(937.6)	(-)	240	(-)	10.9
324.5	(1064.5)	195	520	16.7	9.1
377.8	(1239.2)	595	(-)	8.9	(-)
415.1	(1361.5)	370	190	15.0	30.0
511.7	(1678.4)	40	35	30.9	32.9
555.7	(1822.8)	40	40	34.2	33.7
570.3	(1870.7)	55	50	29.2	29.8
584.1	(1915.8)	125	115	19.0	18.8
602.4	(1976.0)	40	35	32.6	32.7
619.6	(2032.4)	45	(-)	31.6	(-)
649.8	(2131.2)	150	110	24.2	22.6
665.2	(2181.8)	85	70	27.1	27.6
679.4	(2228.5)	50	55	31.6	29.3
700.6	(2298.0)	70	65	25.6	25.9
712.4	(2336.8)	110	80	26.2	25.9
726.1	(2381.6)	165	95	20.9	21.0
742.7	(2436.1)	85	80	25.2	25.5
755.5	(2478.0)	60	90	25.3	23.9
769.4	(2523.7)	70	60	23.4	22.8
785.9	(2577.7)	285	145	18.6	18.4
804.1	(2637.5)	770	360	10.7	11.4
821.5	(2694.6)	50	(-)	23.9	(-)
829.1	(2719.5)	345	240	22.7	24.1
861.7	(2826.2)	90	95	28.2	27.8
871.0	(2856.8)	130	115	20.8	20.5
895.9	(2938.6)	180	150	19.2	18.7
908.5	(2979.8)	390	155	14.8	18.7

Table 5. Water permeabilities measured on vertically and horizontally oriented core samples obtained from the USW GU-3/G-3 borehole. Leader (-) indicates sample was not suitable for measurement.

Sample depth in meters	(feet)	Permeability range in microdarcies Vertical	Horizontal
16.6	(54.2)	0.67	9.90 - 8.95
29.4	(96.3)	1.61 - 0	0
48.4	(158.8)	0	1.31 - 0.68
63.3	(207.5)	0	85.8 - 0.91
78.4	(257.0)	0.94 - 0.75	1.56 - 0
93.2	(305.7)	0.82	3.72 - 3.62
113.1	(370.9)	155000 - 126000	74400 - 60000
132.7	(435.2)	420 - 420	1420 - 1100
140.6	(461.1)	380 - 340	940 - 885
168.4	(552.3)	8.32 - 8.38	9.20 - 7.04
175.6	(576.0)	4.60 - 3.90	(-)
186.1	(610.3)	2.0 - 0.69	(-)
201.3	(660.3)	200 - 195	550 - 215
217.6	(713.8)	2.37 - 0.75	(-)
233.2	(765.0)	0.70	(-)
251.7	(825.6)	0.13 - 0.057	0
269.5	(884.1)	72.4 - 87.3	(-)
282.0	(925.0)	0.15 - 0.015	8.80 - 0.021
292.0	(957.7)	0.96 - 0.48	15.1 - 10.4
321.9	(1055.8)	0	0
338.1	(1108.9)	0.42	59.3 - 9.80
355.5	(1165.9)	0	95.0 - 1.80
		reversed flow	82.1 - 1.02
369.9	(1213.2)	2.75 - 0.05	135 - 6.35
384.7	(1261.8)	0	20.3 - 1.86
399.7	(1310.9)	5410 - 5150	10000 - 7610
457.9	(1501.8)	31300 - 24600	39200 - 26300
499.3	(1637.7)	52000 - 49000	45800 - 42000
508.1	(1666.7)	9150 - 8440	10100 - 9180
520.3	(1706.6)	2440 - 2270	2280 - 2190
542.6	(1779.6)	235000 - 200000	(-)
552.9	(1813.5)	160 - 145	(-)
569.2	(1866.9)	39.3 - 31.8	37.8 - 14.1
583.1	(1912.7)	13.0 - 8.76	(-)
597.1	(1958.4(	15.0 - 12.5	(-)
612.3	(2008.4	(-)	103 - 22.3
632.6	(2075.0)	11300 - 10700	(-)
643.3	(2110.0)	248 - 190	11.1 - 10.8
660.8	(2167.5)	170 - 86.3	370 - 199
688.0	(2256.8)	0	1.47 - 0.55
705.8	(2315.0)	0	0.93 - 0.65
718.5	(2356.7)	2.06 - 1.83	5.20 - 0.99
733.9	(2407.2)	1.14	0
752.6	(2468.5)	0.17	1.37 - 1.14
768.8	(2521.5)	7.46 - 2.82	7.11 - 7.17
781.2	(2562.4)	395 - 380	(-)
798.0	(2617.5)	0.21	255 - 120
811.1	(2660.5)	36200 - 31200	8.36 - 6.21
832.6	(2730.9)	670 - 600	905 - 680
845.0	(2771.7)	720 - 715	480 - 370

Table 5 (continued)

859.1	(2817.7)	140 - 130	98.2 - 99.1
874.5	(2868.2)	98.5 - 96.7	140 - 131
888.3	(2913.6)	9.59 - 7.63	48.5 - 20.0
910.4	(2986.1)	1.44 - 1.20	5.40 - 5.40
915.9	(3004.1)	16.5 - 15.6	28.0 - 8.18
933.5	(3062.0)	2.45 - 1.04	2.82 - 2.88
949.8	(3115.4)	0.53 - 0.45	0.90 - 0.69
963.3	(3159.6)	2.08	1.50 - 0.63
986.3	(3235.0)	0.58 - 0.32	1.19 - 0.39
1009.4	(3310.7)	8.10 - 4.0	6.04 - 5.88
1024.5	(3360.3)	3.34 - 2.81	8.54 - 1.95
1040.0	(3411.2)	2.20 - 1.06	1.07 - 1.04
1056.1	(3463.9)	13.5 - 2.0	2.04 - 1.50
1070.5	(3511.2)	1.73 - 1.14	5530 - 4910
1085.4	(3560.2)	370 - 140	10.9 - 5.30
1101.0	(3611.3)	0.58 - 0.53	15.5 - 9.0
1115.6	(3659.3	1.68 - 1.02	3.86 - 2.71
1165.5	(3822.7)	0.22	107 - 55
1177.2	(3861.2)	(-)	0.28 - 0.35
1192.8	(3912.3)	0.78 - 0.44	0
1207.5	(3960.5)	3.0 - 1.44	0
1222.3	(4008.9)	5.25 - 1.32	15.6 - 11.9
1237.4	(4058.7)	265 - 154	80 - 62
1253.2	(4110.6)	5.94 - 1.56	4.9 - 1.5
1268.0	(4159.0)	0.71 - 0.52	16.1 - 1.90
1283.4	(4209.5)	(-)	48.0 - 1.35
1299.1	(4261.0)	322 - 285	188 - 133
1314.6	(4311.8)	17.9 - 4.55	43.1 - 22.2
1329.6	(4361.0)	(-)	29.7 - 0.20
1344.5	(4409.9)	(-)	30.8 - 5.86
1392.6	(4567.8)	2.59 - 0	9.58 - 4.80
1420.7	(4659.9)	130 - 102	30.3 - 9.62
1435.3	(4707.9)	3.34 - 3.0	8.30 - 4.30
1450.0	(4755.9)	14.7 - 13.5	(-)
1469.1	(4818.6)	319 - 275	265 - 220
1482.0	(4860.8)	2.11 - 0.81	1.52 - 1.25
1497.2	(4910.7)	45.0 - 30.1	18.1 - 10.3
1517.7	(4977.9)	3.21 - 0.35	62.8 - 20.0
1527.4	(5009.8)	27.5 - 15.0	8.84 - 8.36

Table 6. Water permeability values in microdarcies measured on vertically and horizontally oriented core samples from the USW G-4 borehole. Leader (-) indicates sample was not suitable for measurement.

Sample depth in meters	(feet)	Permeability range in microdarcies Vertical	Horizontal
18.0	(59.0)	0	135 - 54.0
27.7	(90.8)	0	88.5 - 1.05
85.5	(280.4)	61.0 - 44.5	920 - 510
101.3	(332.3)	(-)	185 - 185
119.0	(390.3)	52.5 - 45.5	(-)
167.2	(548.4)	(-)	7180 - 5820
183.7	(602.6)	235 - 210	(-)
203.8	(668.6)	97.0 - 62.0	0.62 - 0.06
226.4	(742.5)	0	305 - 0.46
250.4	(821.2)	3.50 - 0	6.60 - 3.40
266.9	(875.5)	0	(-)
285.9	(937.6)	(-)	1.45 - 1.31
324.5	(1064.5)	97 - 90.6	313 - 267
377.8	(1239.2)	0	(-)
415.1	(1361.5)	2.5	19.1 - 18.2
460.8	(1511.4)	595 - 565	(-)
511.7	(1678.4)	14.6 - 10.8	(-)
555.7	(1822.8)	4190 - 3970	7680 - 7460
570.3	(1870.7)	2480 - 1930	4600 - 4540
548.1	(1915.8)	70.0 - 52.0	26.1 - 26.0
602.4	(1976.0)	120 - 110	22.3 - 12.7
619.6	(2032.4)	51.4 - 45.4	(-)
649.8	(2131.2)	36.2 - 32.6	70.7 - 38.9
665.2	(2181.8)	43.2 - 33.5	210 - 184
679.4	(2228.5)	650 - 525	32.0 - 22.1
700.6	(2298.0)	1640 - 1490	2310 - 2020
712.4	(2336.8)	2220 - 2070	3210 - 3140
726.1	(2381.6)	365 - 345	520 - 450
742.7	(2436.1)	4190 - 4060	4110 - 4020
755.5	(2478.0)	7120 - 6950	6310 - 5480
769.4	(2523.7)	2900 - 2700	2630 - 2330
785.9	(2577.7)	12.7 - 11.1	340 - 18.0
804.1	(2637.5)	2.34 - 1.40	21.4 - 5.90
821.5	(2694.6)	(-)	85.8 - 6.80
829.1	(2719.5)	850 - 585	7530 - 6780
861.7	(2826.2)	27.9 - 23.6	120 - 89.1
871.0	(2856.8)	46.5 - 38.6	56.5 - 44.3
895.9	(2938.6)	26.0 - 21.5	55.2 - 43.3
908.5	(2979.8)	18.0 - 15.3	290 - 230

References Cited

Anderson, L.A., 1981, Rock property analysis of core samples from the Yucca Mountain UE25a-1 borehole, Nevada Test Site, Nevada: U.S. Geological Survey Open-File Report 81-1338, 36 p.

Anderson, L.A., 1984, Rock property measurements on large-volume core samples from the Yucca Mountain USW GU-3/G-3 and USW G-4 boreholes: Nevada Test Site, Nevada: U.S. Geological Survey Open-File Report 84-552, 39 p.

Brace, W.F., and Orange, A.S., 1968, Electrical resistivity changes in saturated rocks during fracture and frictional sliding: Journal of Geophysical Research, v. 73, no. 4, p. 1433-1445.

Brace, W.F., 1977, Permeability from resistivity and pore shape: Journal of Geophysical Research, v. 82, no. 23, p. 3343-3349.

Carr, W.J., Byers, F.M., and Orkild, P.P., 1984, Stratigraphic and volcano-tectonic relations of Crater Flat Tuff and some older volcanic units, Nye County, Nevada: U.S. Geological Survey Open-File Report 84-114, 42 p.

Carr, M.D., Wadell, S.J., Vick, G.S., Stock, J.M., Monsen, S.A., Harris, A.G., Cork, B.W., and Byers, F.M., 1986, Geology of drillhole UE25p#1 - A test hole into pre-Tertiary rocks near Yucca Mountain, southern Nevada: U.S. Geological Survey Open-File Report 86-175, 87 p.

Keller, G.V., and Frischnecht, F.C., 1966, Electrical methods in geophysical prospecting: Pergamon Press, Oxford, New York, Toronto, p. 35.

Johnson, G.R., 1979, Textural properties, in Hunt, G.R., Johnson, G.R., Olhoeft, G.R., Watson, D.E., and Watson, Kenneth, Initial report of the petrophysics laboratory: U.S. Geological Survey Circular 789, p. 67-74.

Olsen, R.E., and Daniel, D.E., 1981, Measurement of the hydraulic conductivity of fine-grained soils, in Zimmie, T.F., and Riggs, C.O., eds., Permeability and groundwater contaminant transport: American Society for Testing and Materials, Special Technical Publication 746, p. 18-64.

Scott, R.B., and Castellanos, M., 1984, Stratigraphic and structural relations of volcanic rocks in drill holes USW GU-3 and USW G-3, Yucca Mountain, Nye County, Nevada: U.S. Geological Survey Open-File Report 84-491, 121 p.

Sowers, G.F., 1981, Rock permeability or hydraulic conductivity - an overview, in Zimmie, T.F., and Riggs, C.O., eds., Permeability and groundwater contaminant transport: American Society for Testing and Materials, Special Technical Publication 746, p. 65-83.

Spengler, R.W., and Chornack, M.P., 1984, Stratigraphic and structural characteristics of volcanic rocks in core hole USW G-4, Yucca Mountain, Nye County, Nevada: U.S. Geological Survey Open-File Report 84-789, 77 p.

Winograd, I.J., and Thordarson, William, 1975, Hydrogeologic and hydrochemical framework, south-central Great Basin, Nevada-California, with special reference to the Nevada Test Site: U.S. Geological Survey Professional Paper 712-C, 126 p.

Figure 1. Map of the Yucca Mountain study area showing the locations of the USW GU-3/G-3 and USW G-4 boreholes and the J-13 water drillhole.

Figure 2. Dry bulk density values for USW GU-3/G-3 horizontally and vertically oriented samples plotted as a function of sampling depth. The unlabeled intervals in the stratigraphic column are bedded ash-fall tuffs (Scott and Castellanos, 1984).

Figure 3. Saturated bulk density values for USW GU-3/G-3 horizontally and vertically oriented samples plotted as a function of sampling depth. The unlabeled intervals in the stratigraphic column are bedded ash-fall tuffs (Scott and Castellanos, 1984).

Figure 4. Grain density values for USW GU-3/G-3 horizontally and vertically oriented samples plotted as a function of sampling depth. The unlabeled intervals in the stratigraphic column are bedded ash-fall tuffs (Scott and Castellanos, 1984).

Figure 5. Porosity values for USW GU-3/G-3 horizontally and vertically oriented samples plotted as a function of sampling depth. The unlabeled intervals in the stratigraphic column are bedded ash-fall tuffs (Scott and Castellanos, 1984).

Figure 6. Resistivity values for USW GU-3/G-3 horizontally and vertically oriented samples plotted as a function of sampling depth. The unlabeled intervals in the stratigraphic column are bedded ash-fall tuffs (Scott and Castellanos, 1984).

Figure 7. Dry bulk density values for USW G-4 horizontally and vertically oriented samples plotted as a function of sampling depth. The unlabeled intervals in the stratigraphic column are bedded ash-fall tuffs (Spengler and Chornack, 1984).

Figure 8. Saturated bulk density values for USW G-4 horizontally and vertically oriented samples plotted as a function of sampling depth. The unlabeled intervals in the stratigraphic column are bedded ash-fall tuffs (Spengler and Chornack, 1984).

Figure 9. Grain density values for USW G-4 horizontally and vertically oriented samples plotted as a function of sampling depth. The unlabeled intervals in the stratigraphic column are bedded ash-fall tuffs (Spengler and Chornack, 1984).

Figure 10. Porosity values for USW G-4 horizontally and vertically oriented samples plotted as a function of sampling depth. The unlabeled intervals in the stratigraphic column are bedded ash-fall tuffs (Spengler and Chornack, 1984).

Figure 11. Resistivity values for USW G-4 horizontally and vertically oriented samples plotted as a function of sampling depth. The unlabeled intervals in the stratigraphic column are bedded ash-fall tuffs (Spengler and Chornack, 1984).

Figure 12. Diagram of the stainless steel sample holder used for permeability measurements. Porous teflon spacers, T, are designed to direct water flow uniformly through the sample, S, under confining pressure, Pc, and driving pressure, Pd, of 100 and 50 psi, respectively. The capillary tube is used to measure the rate of water flow through the rock.

Figure 13. Plot demonstrating a decrease in permeability with time for the USW GU-3 sample from the 355.3 m depth. The initial run, shown by open circles, was made with distilled water as the permeant. The closed circles represent measurements made with a reversed water flow. Water from the Nevada Test Site J-13 water well produced the series of permeability values denoted by triangles.

Figure 14. Initial (maximum) permeability values for USW GU-3/G-3 horizontally and vertically oriented samples plotted as a function of sampling depth. The unlabeled intervals in the stratigraphic column are bedded ash-fall tuffs (Scott and Castellanos, 1984).

Figure 15. Initial (maximum) permeability values for USW G-4 horizontally and vertically oriented samples plotted as a function of sampling depth. The unlabeled intervals in the stratigraphic column are bedded ash-fall tuffs (Spengler and Chornack, 1984).

Figure 16. Pore diameter distribution determined for the vertical (top) and horizontal (bottom) plugs obtained from the USW GU-3 355.3 m core sample. Property values listed for each sample are porosity, ϕ, in percent; grain density, GD, in Mg/m^3; resistivity, ρ, in ohm-m; permeability, k, in microdarcies; and average pore dimension, APD, in microns.

Figure 17. Pore diameter distribution determined for the vertical (top) and horizontal (bottom) plugs obtained from the USW GU-3 140.6 m core sample. Property values listed for each sample are porosity, ϕ, in percent; grain density, GD, in Mg/m^3; resistivity, ρ, in ohm-m; permeability, k, in microdarcies; and average pore dimension, APD, in microns.